Mesh-Enabled Targeting in a GPS-Denied Environment

NPS-SE-26-003

NAVAL POSTGRADUATE SCHOOL

MONTEREY, CALIFORNIA

TECHNICAL REPORT

MESH-ENABLED TARGETING IN A GPS-DENIED ENVIRONMENT

by

Dr. Oleg Yakimenko
Joseph Lukefahr
Ronny Ruben
Jangho Yoon
Dr. Fabian Wilking

March 31, 2026

Prepared for: COMNAVSURFPAC. This research is supported by funding from the Naval Postgraduate School, Naval Research Program (PE 0605853N/2098). NRP Project ID: NPS-25-N137-A.

THIS PAGE INTENTIONALLY LEFT BLANK

REPORT DOCUMENTATION PAGE

Form Approved
OMB No. 0704–0188

1. REPORT DATE *(DD–MM–YYYY)*	2. REPORT TYPE	3. DATES COVERED *(From — To)*
31-MAR-2026	Technical Report	01-APR-2025 to 31-MAR-2026

4. TITLE AND SUBTITLE

MESH-ENABLED TARGETING IN A GPS-DENIED ENVIRONMENT

5a. CONTRACT NUMBER

5b. GRANT NUMBER

5c. PROGRAM ELEMENT NUMBER
0605853N/2098

6. AUTHOR(S)

Dr. Oleg Yakimenko, Joseph Lukefahr, Ronny Ruben, Jangho Yoon, Dr. Fabian Wilking

5d. PROJECT NUMBER
NPS-25-N137-A

5e. TASK NUMBER

5f. WORK UNIT NUMBER

7. PERFORMING ORGANIZATION NAME(S) AND ADDRESS(ES)

Naval Postgraduate School
Monterey, CA 93943

8. PERFORMING ORGANIZATION REPORT NUMBER
NPS-SE-26-003

9. SPONSORING / MONITORING AGENCY NAME(S) AND ADDRESS(ES)

Commander, Naval Surface Force, U.S. Pacific Fleet
Naval Research Program

10. SPONSOR/MONITOR'S ACRONYM(S)
COMNAVSURFPAC
NRP

11. SPONSOR/MONITOR'S REPORT NUMBER(S)
NPS-25-N137-A
NPS-SE-26-003

12. DISTRIBUTION / AVAILABILITY STATEMENT

Distribution Statement A. Approved for public release: Distribution is unlimited.

13. SUPPLEMENTARY NOTES

The views expressed in this document are those of the authors and do not reflect the official policy or position of the Department of Defense or the U.S. Government.

14. ABSTRACT

Adversary jamming, long-range sensing, and space denial capabilities increasingly threaten U.S. and allied command-and-control operations across the Pacific theater. These contested environments degrade traditional GPS and SATCOM based kill chains and amplify the need for resilient, distributed sensing and targeting architectures. This study integrates analytical modeling, system architecture development, energy-aware clustering algorithms, decentralized swarm-control methods, communication range analysis, and hardware-in-the-loop flight experimentation. Results show that while mesh-networked unmanned aerial system swarms offer substantial resilience advantages, their functional lifetime is highly sensitive to geometric constraints, energy availability, and clustering strategy. This work establishes a rigorous foundation for mesh-enabled targeting and highlights critical research needs in communications resilience, swarm autonomy, multi-sensor fusion, and operational experimentation to support Distributed Maritime Operations in contested environments.

15. SUBJECT TERMS

mesh network, global positioning system, GPS, GPS-denied environment, unmanned aerial system, UAS, UAS swarm, satellite communications, SATCOM

16. SECURITY CLASSIFICATION OF:			17. LIMITATION OF ABSTRACT	18. NUMBER OF PAGES	19a. NAME OF RESPONSIBLE PERSON
a. REPORT	b. ABSTRACT	c. THIS PAGE			Dr. Oleg Yakimenko
Unclassified	Unclassified	Unclassified	UU	83	19b. TELEPHONE NUMBER *(include area code)* (831) 656-2826

NSN 7540-01-280-5500

Standard Form 298 (Rev. 8–98)
Prescribed by ANSI Std. Z39.18

THIS PAGE INTENTIONALLY LEFT BLANK

NAVAL POSTGRADUATE SCHOOL
Monterey, California 93943-5000

Ann E. Rondeau
President

W. Matthew Carlyle
Acting Provost

The report entitled "Mesh-Enabled Targeting in a GPS-Denied Environment" was prepared for Commander, Naval Surface Force, U.S. Pacific Fleet (COMNAVSURFPAC) and funded by the Naval Postgraduate School, Naval Research Program (PE 0605853N/2098).

Further distribution of all or part of this report is authorized.

This report was prepared by:

Dr. Oleg Yakimenko
Distinguished Professor and Chair
Systems Engineering Department

Joseph Lukefahr
Faculty Associate
Information Sciences Department

Reviewed by:

Dr. Michael Freeman
Vice Provost for Academic Leadership

Released by:

Michael Hesse
Vice Provost for Research & Innovation

THIS PAGE INTENTIONALLY LEFT BLANK

ABSTRACT

Adversary jamming, long-range sensing, and space denial capabilities increasingly threaten U.S. and allied command-and-control operations across the Pacific theater. These contested environments degrade traditional GPS and SATCOM based kill chains and amplify the need for resilient, distributed sensing and targeting architectures. This study integrates analytical modeling, system architecture development, energy-aware clustering algorithms, decentralized swarm-control methods, communication range analysis, and hardware-in-the-loop flight experimentation. Results show that while mesh-networked unmanned aerial system swarms offer substantial resilience advantages, their functional lifetime is highly sensitive to geometric constraints, energy availability, and clustering strategy. This work establishes a rigorous foundation for mesh-enabled targeting and highlights critical research needs in communications resilience, swarm autonomy, multi-sensor fusion, and operational experimentation to support Distributed Maritime Operations in contested environments.

THIS PAGE INTENTIONALLY LEFT BLANK

Table of Contents

THIS PAGE INTENTIONALLY LEFT BLANK

List of Figures

List of Tables

THIS PAGE INTENTIONALLY LEFT BLANK

List of Acronyms and Abbreviations

A2/AD	anti-access/area-denial
C2	command and control
CODE	Collaborative Operations in Denied Environment
CONOPS	Concept of Operations
COTS	commercial off-the-shelf
C-UAS	counter unmanned aerial system
DARPA	Defense Advanced Research Projects Agency
DDIL	denied, degraded, intermittent, and limited
EA	electronic attack
EO/IR	electro-optical/infrared
eVTOL	electric vertical takeoff and landing
EW	electronic warfare
FANET	flying ad hoc network
FPV	first-person view
FW	fixed wing
GPS	Global Positioning System
ISR	Intelligence, Surveillance, and Reconnaissance
LEACH	Low-Energy Adaptive Clustering Hierarchy
LiDAR	Light Detection and Ranging
LPI	low probability of intercept
LPD	low probability of detection
MANET	Mobile Ad Hoc Network
NATO	North Atlantic Treaty Organization
NPS	Naval Postgraduate School
RF	radiofrequency
SATCOM	satellite communications
SBU	Security Service of Ukraine
sUAS	small unmanned aerial system
TDMA	Time Division Multiple Access
UAS	unmanned aerial system
UAV	unmanned aerial vehicle
USV	uncrewed surface vessel
VTOL	vertical takeoff and landing

THIS PAGE INTENTIONALLY LEFT BLANK

1 Background

The rapid proliferation of unmanned aerial systems (UASs) across civilian, criminal, and military domains has driven significant investment in counter unmanned aerial system (C-UAS) technologies. Anti-access/area-denial (A2/AD) strategies seek to prevent adversary entry and freedom of maneuver by integrating layered sensing and fires with electronic warfare (EW), cyber operations, and physical attack against command and control (C2) nodes and communications infrastructure. These systems increasingly integrate multi-spectral sensing, real time data fusion, electronic attack (EA), and kinetic effectors.

1.1 Modern UAS Jammers

Tables 1 and 2 show two representative systems, Aaronia AG (Germany) and Kongsberg Defence & Aerospace (KDA) (Norway) that while pursuing the same objective feature two distinct design philosophies: Aaronia with a primary emphasis on radiofrequency (RF) detection and selective jamming, and Kongsberg with a broader sensor fusion and kinetic centric architecture that may integrate third-party EW modules as needed.

Table 1. Comparative analysis of AARTOS and CORTEX C-UAS system characteristics.

Dimension	**Aaronia AG — AARTOS (DDS + Smart/CMS Jammers) [1], [2], [3]**	**Kongsberg Defence & Aerospace — C-UAS (CORTEX, PROTECTOR, CROWS, DR100) [4], [5], [6], [7]**
Primary C-UAS concept	RF centric detection/identification (protocol decoding, direction- finding/triangulation), extensible with radar/electro-optical and selective jamming effectors	Sensor fusion + networked fire control + kinetic effectors; architecture designed to integrate sensors/weapon stations and (optionally) non kinetic modules, but EW parameters are not openly detailed
Kinetic engagement ranges (published)	AARTOS documentation is primarily RF/EW focused; kinetic effectors depend on third party integrations (not specified in the cited AARTOS sources)	Reported effective engagement >1,000 m with small caliber weapon (0.50 cal) in CORTEX Typhon; CROWS C-UAS reporting cites up to 1,200 m engagement
System integration/scalability	AARTOS supports multi sensor fusion (RF+radar+cameras) and scalable deployments (site/border/large areas)	KDA emphasizes networked C-UAS via ICS and collaborative fire control across multiple platforms/nodes
Representative products (C-UAS)	AARTOS DDS platform; PSJ360 Smart Jammer and other CMS jammer variants	CORTEX Typhon (fielded), PROTECTOR/CROWS C-UAS upgrades, DR100 drone detection radar
Best fit use cases (from open descriptions)	Long range RF warning, protocol identification, operator localization, and soft kill defeat where legally permitted	Mobile formations and protected assets needing networked detection + kinetic response; soft kill as optional integrated layer

Table 2. Comparative analysis of AARTOS and CORTEX C-UAS capabilities.

Dimension	**Aaronia AG — AARTOS (DDS + Smart/CMS Jammers) [1], [2], [3]**	**Kongsberg Defence & Aerospace — C-UAS (CORTEX, PROTECTOR, CROWS, DR100) [4], [5], [6], [7]**
Published detection range (UAS)	Vendor states 40 km consumer / 80 km military for AARTOS DDS in some configurations	Public reporting emphasizes engagement and networking; detection/tracking ranges depend on integrated radars (example radar tracks targets >10 km in a CROWS C-UAS context)
Alternate/variant detection range claims	Datasheets commonly cite up to 50 km detection range (scenario dependent) with 360° dome coverage and height info via 3D DF	DR100 is described as a purpose-built drone detection radar with networked capability; numerical range not stated on the referenced product page
RF detection frequency coverage	RF detection coverage stated as 10 MHz – 8 GHz	KDA sources for the overall C-UAS stack do not publish RF detection bands; some deployments rely on radar bands (e.g., Ku band radar in an example CROWS C-UAS configuration)
Ultra-wideband monitoring (variants)	Some AARTOS materials claim 20 MHz – 20 GHz monitoring (variant dependent)	Not publicly specified for KDA's C-UAS
Direction finding/localization	Real time DF with "height information" and localization of drone/operator in system literature; supports multi sensor integration	Networked approach shares tracks across nodes and cues weapon stations; radar/EO inputs fused via KDA's ICS/CORTEX Typhon
Published jamming range	Programmable "Smart Jammer" class cited at 10 km range	Not publicly specified
Jammer output power (published)	For the PSJ360 - up to 800 W CWP and up to 5 kW EIRP (config dependent)	Not publicly specified
Jamming frequency coverage (published)	For PSJ360 - gapless 400 MHz – 6 GHz programmable; <400 MHz on request	Not publicly specified
Jamming approach (selective vs barrage)	Emphasizes selective, directional/sector jamming to reduce unintended interference; 360° coverage via multiple sectors	Focus is on kinetic defeat and networked cueing; EW integration discussed at high level only
Examples of common target bands addressed	Fixed band jammer literature mentions typical drone bands such as 2.4 GHz, 5.x GHz and GNSS L band	Radar examples include Ku band tracking radar in CROWS C-UAS upgrades; no jammer bands disclosed
Spoofing (GNSS deception)	No clear public product claim of GNSS spoofing; materials highlight jamming/disruption and selective denial	No public claims of GNSS spoofing in cited KDA materials; emphasis is on detection/fusion and kinetic engagement

A review of the public literature indicates that Aaronia AG and Kongsberg represent complementary approaches within the broader C-UAS technology spectrum. Aaronia's AARTOS excels in RF detection and selective jamming, offering quantifiable and publicly documented specifications concerning frequency ranges, detection distances, and output power.

Its systems align closely with research emphasizing early warning RF intelligence, protocol aware detection, and surgical electronic disruption.

Kongsberg, meanwhile, embodies the sensor fusion and kinetic layered defense paradigm, consistent with doctrinal trends in North Atlantic Treaty Organization (NATO) militaries. Its systems prioritize radar centric tracking, network based collaborative fire control, and integration with existing weapon stations, while maintaining flexibility to incorporate EW effectors from external suppliers. The lack of publicly disclosed jamming specifications reflects both operational security considerations and Kongsberg's broader focus on modularity rather than proprietary jammers.

In sum, two representative C-UAS systems of Tables 1 and 2 show two trends – RF based countermeasures and a more holistic, multi-domain C-UAS architecture that can incorporate EW but is not centered on it. Together, these systems illustrate the evolving balance between non-kinetic and kinetic approaches in modern counter drone warfare, as well as the growing importance of interoperable, scalable, networked defense ecosystems capable of addressing both commercial off-the-shelf (COTS) drones and increasingly sophisticated military UASs.

1.2 UAS Operations within a DDIL Environment

In such denied, degraded, intermittent, and limited (DDIL) conditions—where Global Positioning System (GPS) and satellite communications (SATCOM) may be jammed or spoofed—targeting architectures that rely on centralized, continuous connectivity become brittle, and the kill chain is vulnerable to disruption at multiple points. This has contributed to the doctrinal shift from linear "kill chains" toward distributed "kill webs"—multiple redundant paths that connect sensors, decision-makers, and shooters across domains so that the mission can continue even if individual nodes or links are degraded [8], [9].

Within this context, mesh-enabled targeting can be defined as a targeting approach in which heterogeneous nodes (unmanned systems, sensors, relays, and human controllers) collaborate through resilient, multi-path networking and edge autonomy to sustain the find–fix–track–target–engage–assess process despite DDIL constraints and attrition. The key distinction from "networked operations" is the explicit emphasis on (i) graceful degradation,(ii) distributed decision-making and tasking, and (iii) multiple alternative communications and sensing pathways rather than a single exquisite link [10].

Recent operations in the Russo–Ukrainian war provide concrete, contemporary demonstrations of these principles. Operation Spiderweb on 1 June 2025 reportedly involved coordinated strikes against multiple remote Russian air bases using small drones covertly transported and launched from truck-borne containers near targets, enabling a wide geographic strike across multiple time zones and compressing defensive warning time (Figure 1) [11], [12], [13], [14], [15].

(a) (b)

Figure 1. Ukraine drones used to conduct "Operation Spiderweb" (a), stacked inside the truck container (b) [16].

Open-source technical assessments suggest hybrid control mechanisms: pre-planned navigation and telemetry pathways consistent with ArduPilot Mission Planner workflows (including transmission of telemetry over cellular networks) coupled with manual human-in-the-loop terminal guidance for precision. This final guidance is enabled through a relay system located inside the truck. Moreover, reporting indicates that some drones continued to targets using onboard autonomy when links were disrupted, consistent with a mission design that anticipates EW and supports "continue mission" behaviors under intermittent connectivity [12].

A similar evolution is visible in Ukraine's maritime drone operations, which have imposed persistent operational pressure on Russian naval forces and struck defended infrastructure in the Black Sea region. Reuters' analysis describes the operational significance of explosive uncrewed surface vessels (USVs) as low-cost, difficult-to-detect strike systems used against ships and infrastructure [17]. In the case of the Crimean (Kerch) Bridge, open-source reporting on the 2023 strike attributes the attack to sea drones and notes analysts' assessments that such systems may incorporate satellite communications or onboard navigation and use terminal sensing (e.g., optical) for endgame homing—features consistent with mesh-enabled targeting in maritime DDIL conditions) [18].

In June 2025, the Security Service of Ukraine (SBU) reported a third strike on the Crimean Bridge employing underwater explosives to damage bridge supports, and later reporting (2025) described next-generation "Sea Baby" maritime drones with extended range, modern navigation, and large payload capacities, again consistent with increasing autonomy and robustness (Figure 2) [19], [20], [21], [22], [23], [24].

Figure 2. Two versions of Ukraine USV.

Finally, the emergence of multi-domain unmanned teaming underscores the "mesh" concept at the operational level: reporting indicates Ukrainian USVs have launched airborne "bomber drones" to strike targets ashore in Crimea, including radar components, illustrating how a maritime node can position and enable an aerial node, thereby generating new approach vectors and complicating defensive sensor-to-shooter integration. Together, these cases suggest that mesh-enabled targeting is not merely a communications concept; it is an integrated approach spanning communications resilience, distributed sensing, and

edge decision autonomy to keep the targeting cycle functioning within contested A2/AD envelopes.

1.3 Problem Statement and Research Objectives

This research investigates approaches for modeling the technical feasibility of mobile ad hoc drone networks that enable localized targeting and support distributed lethality doctrine [25]. When tactical conditions permit the deployment of off-board sensors, unmanned aerial vehicles (UAVs) offer the advantage of extended targeting reach. Additionally, employing UAVs as communication relays can mitigate adversary anti-scouting measures by using relatively low-power RF links to pass data from sensors to shooters.

This study focuses on addressing two primary research questions:

- Feasibility of mesh-enabled platforms: Can a swarm of drones—or alternatively, modified U.S. naval vessels, aircraft, and other platforms—be equipped with mesh-networking technologies to support targeting and data exchange when traditional C2 infrastructure is denied or degraded?
- Determinants of network effectiveness: What technical factors govern the performance of energy-efficient, self-organizing drone-based mesh networks operating in contested environments? Key considerations include communication range, resilience to jamming, probability of intercept/detection, and energy constraints.

The remainder of this report is organized as follows. Section 2 provides operational context and introduces formal network definitions. Section 3 presents the system architecture linking desired capabilities to system components. Sections 4 and 5 examine the mathematical foundations of linear and mesh networks as applied to relevant operational scenarios. Section 6 evaluates techniques for energy-efficient UAV clustering. Section 7 summarizes flight tests conducted to refine the problem space and collect supporting data. Finally, Sections 8 and 9 present conclusions and future work.

2 Foundations in Collaborative Autonomy, Mesh Networking, and GPS-Denied Operations

Academic and defense research provides several complementary foundations relevant to mesh-enabled targeting. First, Collaborative Operations in Denied Environment (CODE), a Defense Advanced Research Projects Agency (DARPA) program, formalized the need for collaborative autonomy that remains resilient to bandwidth limitations and communications disruptions, enabling multiple unmanned aircraft to operate under supervisory control rather than requiring dedicated operators per platform [26]. CODE's emphasis on modular autonomy and adaptation under attrition and contested communications directly aligns with the decision and resilience requirements of mesh-enabled targeting architectures.

Second, the communications substrate for mesh-enabled targeting builds upon extensive work in UAS ad hoc networks and mesh networking. Survey and research literature highlights that UAS swarms often form flying ad hoc networks (FANETs) with highly dynamic topology and constrained energy and bandwidth, motivating self-organization and robustness through redundancy. Research on hybrid mesh approaches (e.g., combining IEEE 802.11s with long-range links such as LoRa/LoRaWAN) explicitly addresses range–throughput tradeoffs and the value of heterogeneous links—an important design pattern for DDIL operations. Security and resilience issues are similarly central: work on secure mesh connectivity for UAS swarms identifies vulnerabilities across the stack and frames research challenges for operating without centralized infrastructure, an issue that becomes acute when adversaries actively jam, spoof, or exploit control links [27], [28], [29], [30].

Third, mesh-enabled targeting depends on distributed sensing and cooperative estimation, especially when GPS is degraded. Cooperative multi-robot approaches for GPS-denied environments emphasize decentralized planning under uncertainty and limited sharing of processed observations, demonstrating that useful collaboration can be achieved without full-fidelity data exchange. Recent peer-reviewed work proposes air–ground cooperative architectures for navigation and target guidance in GPS-denied environments, combining local sensing with ranging/anchor techniques and edge planning methods, illustrating practical pathways to maintain positioning and guidance when GNSS is unavailable. These efforts align with mesh-enabled targeting's need to maintain track quality and engagement feasibility under denied PNT and intermittent communications [31], [32], [33].

Fourth, at the C2/architecture level, defense analyses argue for a transition to distributed kill webs with diverse communications paths and machine-to-machine data flows, explicitly motivated by adversary strategies that seek to disrupt U.S. kill chains. This architectural argument is consistent with operational experimentation and commentary emphasizing rapid kill-chain closure through integrated networks and edge nodes, reinforcing the need for resilient data movement and distributed decision support [34], [35].

Finally, this research matches other research efforts conducted by the authors that explicitly frames "mesh-enabled targeting" as a response to adversary jamming and space denial, focusing on feasibility of drone mesh networks to enable organic targeting without satellites while reducing detectability. Collectively, these strands—collaborative autonomy, mesh networking, cooperative sensing/estimation, and kill-web C2—establish a strong scholarly and operational foundation for investigating mesh-enabled targeting in A2/AD.

Despite rich work on swarm comms, collaborative autonomy, and GPS-denied navigation, there remains a need for integrated studies that connect (i) mesh network design (connectivity, low probability of intercept (LPI), low probability of detection (LPD), anti-jam), (ii) cooperative sensing/track fusion under uncertainty, and (iii) tasking/engagement policies that preserve mission success probability under DDIL constraints and active adversary disruption—precisely the system-level problem posed by mesh-enabled targeting.

Table 3 outlines three interlocking taxonomic "meshes" for targeting, each serving a distinct purpose and characterized by unique attributes.

Table 3. Targeting "mesh" taxonomy.

Dimension	**Communications Mesh (C-Mesh)**	**Sensing Mesh (S-Mesh)**	**Decision Mesh (D-Mesh)**
Purpose	Maintain connectivity for C2/telemetry/coordination through redundant, multi-path links; enable graceful degradation and alternative routing under jamming or node loss	Distributed detection, identification, localization, and tracking via multiple nodes and cross-domain cueing; fuse observations at the edge or via intermittent aggregation	Distributed tasking and autonomy to keep missions viable when connectivity is intermittent; includes local planning, re-tasking under attrition, and supervisory control constructs
Key attributes	Heterogeneous links (high-throughput vs long-range), self-healing routing, LPI/LPD behaviors, security hardening [27], [29]	Cooperative perception, edge feature sharing (not raw feeds), multi-view geometry, track-quality management under uncertainty, terminal sensing for engagement [29], [32]	Collaborative autonomy, mission continuation logic, decentralized task allocation, rule-based constraints (ROE), human-in-the-loop supervisory patterns [26], [28]

Using the taxonomy of Table 3, recent operational examples presented in Section 1.2 can be mapped as follows.

1. Operation Spiderweb (1 June 2025)
    - C-Mesh: Open source intelligence (OSINT) analysis suggests telemetry/control compatible with cellular networks and Mission Planner workflows, implying use of alternate communications pathways rather than reliance on a single centralized link.
    - S-Mesh: First-person view (FPV) terminal guidance and released strike footage indicate edge sensing and terminal confirmation, i.e., local node-level target discrimination rather than remote-only targeting.
    - D-Mesh: reporting that drones continued along preplanned routes and completed missions when signals were lost is a direct indicator of "mission continuation" autonomy under contested communications.
2. Crimean Bridge Strikes (2023 and June 2025)
    - C-Mesh: 2023 reporting discusses potential satcom and/or navigation systems enabling long-range transit and control in contested maritime environments.
    - S-Mesh: analyst descriptions emphasize endgame sensing (e.g., optical/locator) and precision aim at bridge structures—consistent with terminal sensing and local homing.
    - D-Mesh: the June 2025 underwater explosives attack reflects extended planning and execution requiring navigation autonomy and precise placement of charges on underwater supports, as publicly described by SBU reporting.
3. USV→UAV Layering (Crimea radar strikes, mid-2025)
    - C-Mesh: USVs enabling airborne drone launch suggests forward positioning of a mobile node that can support operations where traditional access is constrained.
    - S-Mesh: aerial payload delivery from maritime platforms implies cross-domain cueing and distributed sensing for target acquisition and strike assessment.
    - D-Mesh: repeated drops/attacks from USV-launched drones implies local sequencing and coordination logic, consistent with distributed task execution.

This research primarily deals with C-Mesh.

THIS PAGE INTENTIONALLY LEFT BLANK

3 CONOPS and System Architecture Development

Let us consider the potential application of two types of networks: a linear network and a swarm network. In the context of this study, a linear network is envisioned as a means to extend RF signal coverage from the area of operation (targeting) to the decision-making element, aka base station (BS). Figure 3 illustrates this concept, in which one or multiple UAS are employed to extend the operational range.

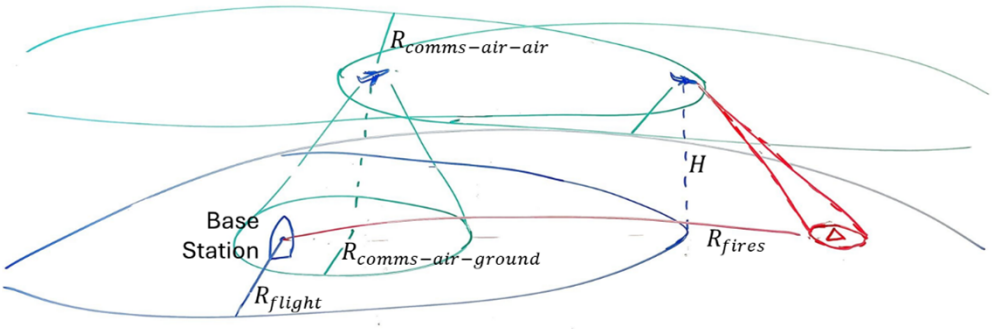

Figure 3. Coverage model of linear network utilizing a single UAS relay.

A swarm network is an ad hoc, decentralized system in which multiple agents (drones or sensors) operate collaboratively, sharing information and coordinating their actions to achieve a common objective. Its topology is inherently dynamic, continuously changing as agents move and interact within the environment. In the scenario illustrated in Figure 4, the primary goal is to extend time on target by dynamically adapting the network architecture to leverage the collective remaining energy (battery) resources while operating in a DDIL environment. Regardless of whether the decision making occurs at a distance—requiring a linear network as depicted in Figure 3—the use of an appropriate network architecture significantly enhances the overall effectiveness and lethality of the drone swarm. The key characteristics of such a network are as follows:

- Adaptive and robust: The system can adapt to changing conditions and failure of individual agents, as control is distributed, not centralized
- Dynamic topology: The network connections and structure are fluid and constantly reconfigure based on local interactions and movement

- Emergent behavior: Complex, collective behaviors emerge from simple local interactions among agents
- Applications: Search and rescue operations, military reconnaissance, complex optimization problems, and providing robust wireless communication in remote or disaster-stricken areas

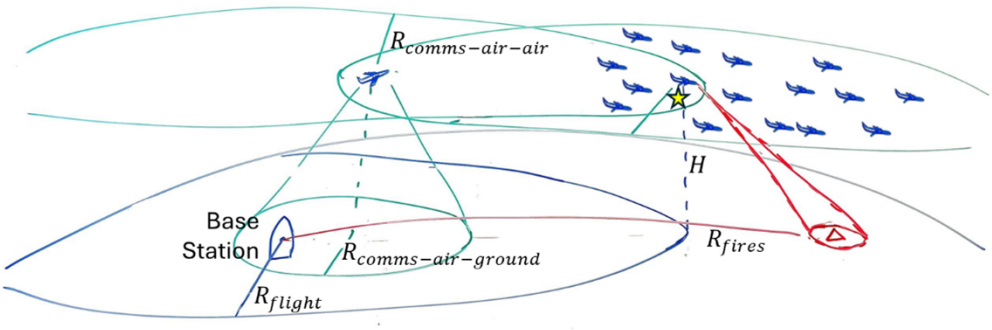

Figure 4. Exploiting a distributed swarm UAS network.

Table 4 compares the key attributes of the two network architectures.

Table 4. Summary of differences between linear and swarm UAS network.

Feature	**Linear Network**	**Swarm Network**
Control	Centralized, rule-based, deterministic	Decentralized, distributed, stochastic
Structure	Fixed, often predefined topology (e.g., tree or linear array)	Dynamic, ad hoc, constantly changing topology
Response	Predictable, linear, proportional to input	Adaptive, emergent, non-linear collective motion
Scalability and robustness	Can have a single point of failure; difficult to scale dynamically	High survivability; scales well by adding or removing agents dynamically

The operational system architecture can be developed using the NATO Architecture Framework v4 (NAFv4), which provides a structured approach for linking desired capabilities to system components. An example of architecture shown Figure 5 emphasizes the definition

of Concept Views (C1–C2, C7–C8, CR), Logical Views (L1–Lr), and a preliminary Physical Allocation diagram. The overarching capability—assured positioning, navigation, and targeting in contested environments—was further decomposed into supporting capabilities.

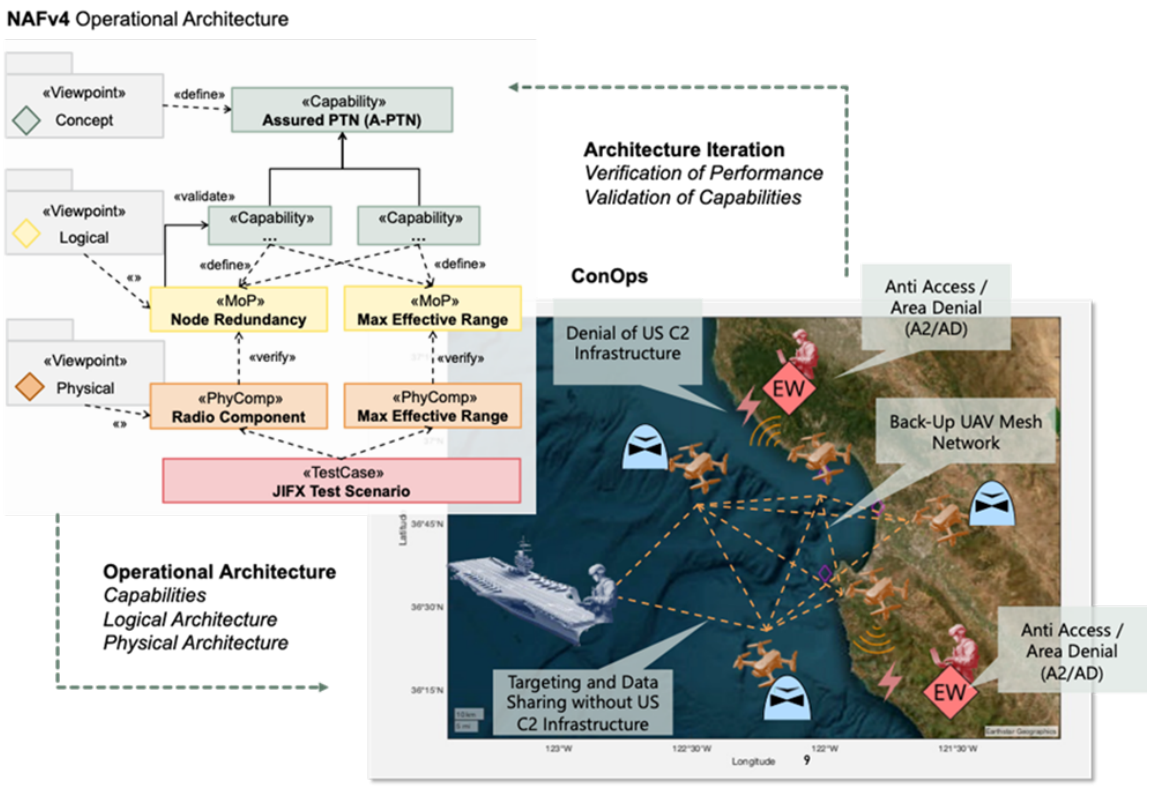

Figure 5. NAFv4 Architecture of the UAS-based mesh network.

Examples of measures of effectiveness to be assessed during subsequent field tests include maximum range of resilient communication, signal integrity, node redundancy, and environmental resilience (e.g., EMI tolerance). Environmental constraints specific to the Pacific theater—such as long-distance missions across island chains and prolonged exposure to humid, saline, and corrosive conditions—were integrated into the architectural considerations as well.

THIS PAGE INTENTIONALLY LEFT BLANK

4 Representative Multirotor and Fixed-Wing UAS

As representative platforms, this study examines two small UAS (sUAS): a Group 1 multirotor (MR) system—the GreenSight Dreamer (Figure 6a)—and a Group 2 fixed-wing (FW) system—the Trinity Pro from Quantum Systems (Figure 6b). Both aircraft are available at the Naval Postgraduate School (NPS) and are widely employed in UAS-related research activities. Their key technical specifications are summarized in Table 5.

(a) (b)

Figure 6. GreenSight Dreamer MR sUAS (a), and Quantum Systems' Trinity Pro FW sUAS.

Table 5. Technical data on Dreamer and Trinity Pro sUAS.

Parameter	**Dreamer MR sUAS**	**Trinity Pro FW sUAS**
Max. take–off weight	< 2 kg (< 4.4 lb)	5.75 kg (12.68 lb)
Max. flight time	24 min (0.4 hr)	90 min (1.5 hr)
Max. flight altitude (MSL)	n/a (subject to command and control range)	5,500 m (18,045 ft)
Command and control range	2 km	5 - 7.5 km (3.1 - 4.7 mi)
Optimal cruise speed	5 m/s (18 km/h or 9.72 kn)	17 m/s (62.1 km/h or 33 kn)

The GreenSight Dreamer is a lightweight (approx. 2 kg), NDAA-compliant multirotor UAS designed for long-endurance aerial imaging and automated inspection missions [36]. It is capable of up to 60-minute flight t imes, p ositioning i t a mong t he highest-endurance quadrotor platforms in its class. The Dreamer is typically equipped with a specialized

multispectral camera payload engineered for rapid, high-quality data collection, and it supports visual, NDVI, and thermal imaging solutions integrated into GreenSight's analytics workflow. Originally developed for agronomic and turf-management applications—where daily automated flights collect visual, multispectral, and thermal data over 300+ acres—the Dreamer has also been adopted for defense-related missions. It forms the core of systems such as GreenSight's Aerial Automated Runway Inspection and Safety Scanner technology platform, where its imaging payload enables rapid detection of foreign object debris, cracks, and vegetation on airfields. The aircraft has been vetted by the U.S. Army Engineer Research and Development Center (ERDC) for National Defense Authorization Act (NDAA) compliance and has been operated in military environments including Fort Carson and NPS Test Range at Camp Roberts, CA. It supports straightforward integration with third-party hardware, including mesh-networking radios.

Quantum Systems' Trinity Pro is a next-generation electric vertical take-off and landing (eVTOL) fixed-wing mapping UAS designed for long-endurance missions (up to 90 minutes) and high-precision geospatial data collection [37]. It features the Quantum-Skynode autopilot with enhanced onboard computing and storage, enabling advanced payload integration and future AI-driven capabilities. One of the platform's defining strengths is its large selection of easily swappable sensors, enabled by a quick-lock payload bay. Trinity Pro supports red/green/blue (RGB), oblique, multispectral, and LiDAR payloads, with sensors integrated seamlessly into QBase 3D for mission planning. The list of specific sensors compatible with the aircraft, includes the Sony RX1R II (42 MP full-frame RGB), Sony UMC (20.1 MP APS-C RGB), MicaSense RedEdge-P (five-band multispectral), MicaSense Altum-PT (multispectral + thermal), and Oblique D2M cameras. The platform also supports geospatial LiDAR such as the Qube 240 (240k points/sec) and the newer Qube 640, developed with YellowScan, offering up to a 176° field of view for corridor and vertical scanning applications [37], [38].

This combination of modular payloads, long endurance, and onboard processing makes Trinity Pro suitable for a wide range of applications including mapping, corridor surveys, agriculture, environmental monitoring, and defense-related ISR roles. The only caveat is that this drone neither transmits any collected imagery back to the ground station nor allows any interaction with its autopilot.

NPS also possesses a more advanced UAS by Quantum Systems, Twister (Figure 7) [39]. It is a compact, backpack portable eVTOL small UAS designed for short-range tactical ISR at the squad and platoon level. The aircraft weighs approximately 3.8–4 kg, can be deployed by a single operator in under two minutes, and provides up to 90 minutes of endurance with an operational range of 15 km [40]. Similar to Trinity Pro, it uses electrically powered vertical takeoff architecture, enabling launch and recovery from confined or concealed positions without catapults or additional ground equipment. Twister carries a modular payload system that, in its baseline configuration, includes the Nighthawk2 EO/IR optical module with day and thermal channels; payloads can be swapped in the field and may include powerful LiDAR for terrain mapping or acoustic sensors for enhanced detection. Designed for stealth and frontline survivability, the UAS features an ultra-low noise signature and onboard edge AI processing (via NVIDIA Jetson Orin NX) for real-time scene analysis and autonomous target classification, transmitting only relevant data to reduce operator load. Twister has been promoted as a complement to Quantum Systems' larger Vector UAS and is already in service with European militaries; in 2025–2026 it was selected by the Bundeswehr as the successor to the ALADIN close-range reconnaissance system, with procurement plans for up to 747 systems [41].

Figure 7. Quantum Systems' Twister sUAS.

As a representative example of a UAS-borne mobile ad hoc networking (MANET) system, let us consider the Rajant radio platform, which operates in two frequency bands—2.4 GHz and 5 GHz (Table 6).

Table 6. Technical characteristics of representative UAS-mounted MANET radio system [42], [43].

Parameter	**Notation**	**Rajant DX2-24**	**Rajant DX2-50**
Transmitter output power (dBm)	P_{TX}	30	27
Transmitter antenna gain (dBi)	G_{TX}	4	4
Receiver antenna gain (dBi)	G_{RX}	4	4
Receiver sensitivity (dBm)	S_{RX}	-100 to -76	-96 to -76
Center frequency (GHz)	f	2.4	5

Rajant's DX2-24 and DX2-50 radios are ultra-lightweight members of the BreadCrumb DX2 series, engineered for highly mobile mesh networking across drones, autonomous vehicles, and other low- Size, Weight, and Power (SWaP) robotic platforms. Both variants share the same core architecture: a single-transceiver, multiple-input and multiple-output (MIMO) antenna mesh node housed in a 123-gram magnesium enclosure, enabling deployment on small UAS and swarm platforms with minimal payload burden. The DX2 series uses Rajant's patented InstaMesh protocol, which provides fully distributed, Layer-2 mobile ad hoc networking with seamless multi-hop routing and continuous path optimization—ideal for environments with constant movement or rapidly changing topology. Both radios achieve data rates up to 300 Mbps and support strong cryptographic options, Wi-Fi access point services for COTS device integration, and fast off-loading v ia E thernet u sing Rajant's Automatic Protocol Tunneling (APT). These characteristics make the DX2-24 and DX2-50 well-suited for resilient, low-latency communications in drone swarms, telematics, remote CCTV, and other applications requiring compact, rugged, and fully mobile mesh nodes. For this research GreenSight Dreamer was integrated with these radios to verify the developed algorithms.

5 Coverage Model of Linear Chain of UAS Relay Nodes

This section presents the foundational analytical framework for multi-sUAS cooperative operations in linear relay configurations. It begins by introducing baseline kinematic and communications models that define the operational limits of individual relay nodes and the aggregate performance of the chain. These models establish the quantitative relationships among endurance-limited operating range, air-to-air and air-to-ground communications constraints, and achievable relay distance. Building on this foundation, the section then transitions to the practical problem of deploying a linear chain of UAS relay nodes, examining feasible delivery and staging concepts that enable nodes to reach prescribed positions while still meeting required time-on-station and communications constraints.

5.1 Connecting Sensor to Shooter

The operating range of the n-th UAS in the sUAS swarm, p_n, required to transmit target tracks of sufficient quality from sensor to shooter base station (Figure 3), can be expressed as

$$p_n = 0.5V_n(T_n - T_s) \tag{1}$$

In this equation, V_n is the UAS's speed, T_n is the available flight time, and T_s is the required time on station. Figure 8 illustrates the computed operating range for two representative sUAS of Table 5 as a function of the required time on station.

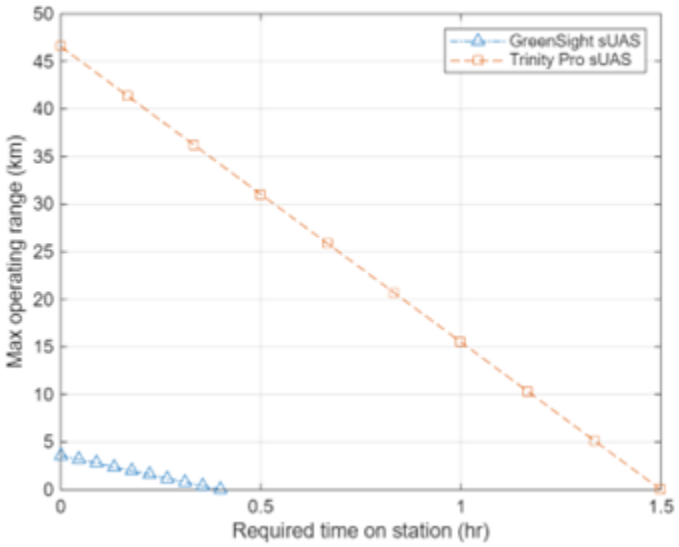

Figure 8. Max operating range of two representative Group 2 sUAS vs. time on station requirement.

As seen in this figure, the effective operating range of MR-class sUAS is very limited. Consequently, Ukrainian SBU units employ a "lay wait, then attack" tactic, which maximizes the time on station (T_n) by remaining in passive listening mode and effectively reduces the sensor transmission time (T_s) to zero. This involves using pre-positioned boxes of FPV drones that are activated when a target is identified by a reconnaissance drone.

The air-to-air communications range of the MANET-equipped n-th UAS, c_n , can be defined in many ways. Let us use the link budget equation defining the link margin M in [44] as

$$M = P_{TX} + G_{TX} - L_{TX} - L_{FS} - L_M - L_{RX} + G_{RX} - S_{RX} \tag{2}$$

In this equation, L_{TX} are the transmitter losses (e.g., due to connectors), L_{FS} is the free-space loss, L_M are the miscellaneous losses (e.g., multipath), L_{RX} are the receiver losses (e.g., due to connectors), while P_{TX}, G_{TX}, G_{RX}, and S_{RX} are defined in Table 6.

In Equation 2, the free-space loss, L_{FS} in [44] is defined as

$$L_{FS} \approx 92.45 + 20 \log_{10} c_n + 20 \log_{10} f \tag{3}$$

where f is the center radiofrequency. Equations 2 and 3 can be used to derive a max communications range, determined by making

$$M = 0 \tag{4}$$

which means the distance at which there is no link margin, or rather, the distance at which received power is at a minimum for usable data transmission. In addition to that, the assumptions about signal loss can be simplified by combining transmitter and receiver loss terms in Equation 2 into a single miscellaneous loss term L_M. Combining Equations 2, 3, and 4 yield

$$0 = P_{TX} + G_{TX} - L_{FS} - L_M + G_{RX} - S_{RX} \tag{5}$$

Rearranging this equation with respect to L_{FS}, substituting the result into Equation 3, and solving for c_n, yields

$$c_n \approx 10^{0.05(P_{TX}+G_{TX}-L_M+G_{RX}-S_{RX}-92.45-20\log_{10} f)} \tag{6}$$

Using the Rajant DX2 MANET parameters from Table 6 for the two representative UASs listed in Table 5 yields the results shown in Figure 9.

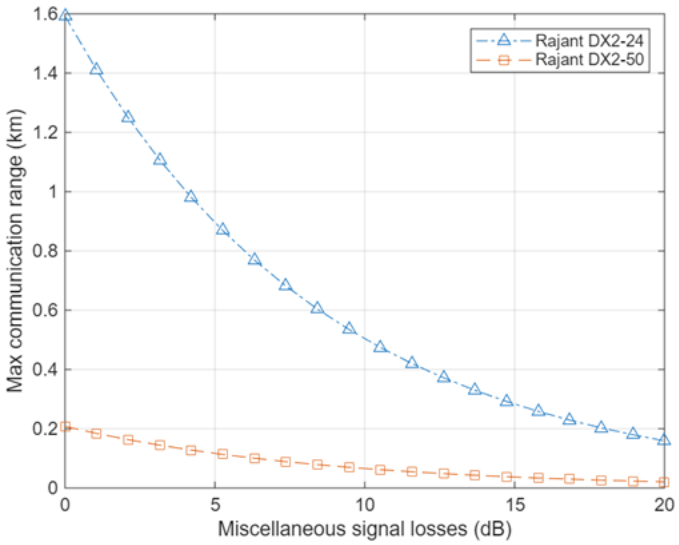

Figure 9. Max communications range of Rajant DX2 radios, given varying miscellaneous signal losses.

As shown in the figure, the Rajant radio does not substantially extend the operating range in the linear network configuration (Figure 3), but it is suitable for exploring the mesh-network concept (Figure 4).

Next, let us consider the communication range of the UAS closest to the shooter, which maintains communication with the shooter via an air-to-ground link, c_0. This range can be modeled in terms of coverage area. One suitable candidate for the air-to-ground propagation model is presented in [45] as

$$c_0 \approx \sqrt{\frac{R(d^2 - H^2)}{R + H}} \tag{7}$$

Here, d is the maximum propagation distance of the relay signal, typically obtained from a link-budget analysis, so that $c_n = d$, R is the Earth's radius (6,370 km), and H is the UAS flight altitude.

Using the Rajant DX2 radio as an example and assuming 4.0 dBi in miscellaneous signal loss, the resulting communication range can be computed as shown in Figure 10.

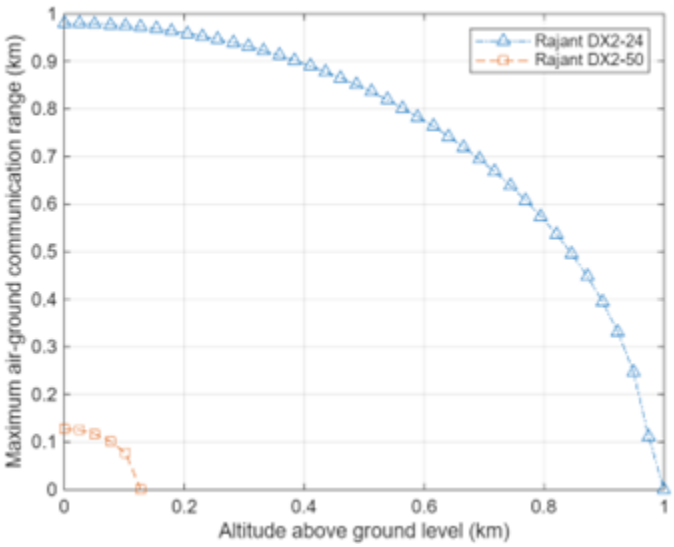

Figure 10. Max air-to-ground communications range of Rajant DX2 radios vs. varying altitude.

To summarize the findings, consider a linear chain of UASs providing a communications relay from a remote sensor that has detected a target. Given n sUASs deployed in series to establish this relay, the total achievable range, r_n, can be estimated as

$$r_n = \begin{cases} \min(c_n, p_n) & n = 0 \\ \min(r_{n-1} + \min(c_n, c_{n-1}), p_n) & n > 0 \end{cases} \tag{8}$$

(This function does not account for the distance from the remote sensor to the target.)

With this formulation, and given a fixed set of organic UASs, we can search for the optimal sequence of UAS deployments that maximizes r_n. Monte Carlo Tree Search (MCTS) may be a suitable algorithm for exploring the deployment permutations due to its efficiency in large combinatorial decision spaces.

Finally, feasibility can be assessed by comparing the resulting relay range against (i) the required distance to the target area and/or (ii) the effective engagement range of the ship's surface-to-surface weapon systems.

5.2 Transit Time and Delivery Concepts

Mesh networking can extend communication range and robustness, but for multirotor UAS with limited onboard energy, a central challenge remains: how to position nodes at prescribed locations along a linear chain without expending the battery needed for time on station. In a relay formulation, the operating range p_n (cf. Eq. 1) implicitly assumes that each node self deploys from the base to its assigned station and still satisfies the required on station time T_s. If the transit leg consumes (nearly) all of the battery, then the linear chain becomes infeasible even when the radio link budget admits a solution.

Therefore each node's energy and time budget is decouple into two legs:

- Delivery leg: how the aircraft reaches its assigned ground range x_n from BS—not necessarily by flying under its own power for the entire distance.
- Duty leg: the required on station time $T_{s,n}$ (and occasional micro repositions) to maintain link geometry and margins.

Let $T^{air}_{transit,n}$ denote the time node n spends actually flying under its own power prior to commencing station keeping. Defining T_n as the aircraft's available endurance (energy limited flight time) for the mission segment, the feasibility constraint is

$$T^{air}_{transit,n} + T_{s,n} \leq T_n \tag{9}$$

All existing communications feasibility checks (Eqs. 2, 3, 4, 5, 6, 7 and the recurrence for r_n in Eq. 8) continue to apply. The logistics problem is thus transformed into minimizing the self-powered transit burden subject to those constraints:

$$\text{Minimize } T^{air}_{transit,n} \tag{10}$$

A set of practical delivery concepts that enable UAS nodes to reach predetermined chain positions—while satisfying both time-on-station and communications feasibility constraints—is outlined below.

1. Ship/Vehicle Pre Positioning with Vertical Insert

- Concept. Move UAS airframes and batteries by ground vehicle or surface vessel (or a small UAS "mothership"), then vertically launch each node near its final station (e.g., within 2–3 min of flight to the final hold).
- Rationale. By reducing $T_{s,n}$ to near zero, nearly the full $T^{air}_{transit,n}$ budget is preserved for on-station duty.
- Implementation Example. In a littoral/island chain setting, a RHIB or unmanned surface vessel moves parallel to shore, stopping at pre-computed GPS waypoints; from each stop, a multirotor (MR) ascends to its assigned altitude and hold.

2. Carrier Assisted Aerial Delivery (FW → MR "Parasite")
    - Concept. Use a long-endurance eVTOL FW platform to airlift one or more MRs near their stations, release, and then proceed to the next drop or return.
    - Rationale. The FW carrier's higher cruise speed and superior specific energy per kilometer covers the long-reach transit; the MR preserves nearly 100% of its battery for $T_{s,n}$.
    - Practical Considerations. FW platforms with 90 min endurance and 17 m/s cruise provide about 90 km still air range budgets. Even accounting for vertical segments, the carrier can step along a linear chain and drop nodes at prescribed points. Quiet airframes with onboard compute can support precision release and pre-drop checks.
    - Mechanics. A simple latch and drop or micro winch mechanism suffices. Upon release, the MR auto stabilizes, then climbs tens of meters to its designated hold.
3. Staging Caches with Field Battery Swaps (Including Hot Swap Packs)
    - Concept. Pre-position weatherproof battery caches (or "nano FOB" cases) proximate to holds. The UAS performs a brief landing for a hot swap and relaunches; alternatively, a ground agent performs the swap.
    - Rationale. When self-deployment is a short hop yet still insufficient, a single planned battery exchange dramatically extends effective reach with minimal added complexity.
    - Variant. Power beacons: a small mast with solar/battery/tether that allows the MR to perch and recharge for 15–30 min before ascending to hold with a near full pack.
4. Tethered Relay Masts / Balloon Mast Inserts

- Concept. For one or two "anchor" nodes near the BS or at critical choke points, employ a tethered quadcopter or a helium balloon mast carrying the radio payload.
- Rationale. This removes time on station energy limits for the hardest nodes, converting them into deterministic infrastructure and easing constraints on the remainder of the chain.

5. Hop by Hop "Leapfrog" Staging
   - Concept. Temporarily form a shorter spacing relay, then advance the farthest node to its final station while nearer nodes maintain the link; repeat outward in a leapfrog fashion.
   - Rationale. Each move entails only small transit distances, maintaining communications coverage throughout setup and keeping $T^{air}_{transit,n}$ modest for all nodes.
   - Note. This can be combined with carrier assist for the farthest or most energy critical legs.
6. Recover and Reseed Rotations to Extend Operations
   - Concept. As any node approaches return to base (RTB) threshold, a carrier (FW) or service vehicle inserts a fresh node at that station; the expended node is recovered for recharge/refit.
   - Rationale. This rotation enables hours long linear chains in denied, degraded, intermittent, and limited (DDIL) environments with limited organic assets.

6 Energy-Efficient Clustering

Operating in an A2/AD environment places significant constraints on UAS swarms. Degraded communication—whether caused by jamming, electromagnetic interference, or the need to meet low-probability-of-intercept requirements—forces UASs to operate at reduced inter-vehicle distances to maintain reliable C2 links. This tighter formation, combined with contested airspace and limited onboard energy reserves, amplifies the need to minimize power consumption across the swarm. Consequently, energy-aware routing becomes essential, with optimal clustering emerging as a key strategy for balancing connectivity, resilience, and overall efficiency.

By intelligently partitioning the swarm into clusters that continue to support primary mission objectives (e.g., ISR) and by assigning cluster heads (CHs) to handle energy-intensive communication tasks such as data aggregation, scheduling, and long-range forwarding, the network reduces redundant transmissions, extends operational endurance, and preserves mission effectiveness under A2/AD constraints. Because CHs perform additional receive/aggregate/transmit operations, they deplete energy more rapidly than regular member nodes, making both CH selection and periodic CH role rotation critical mechanisms for extending network lifetime and ensuring fairness [46], [47], [48].

6.1 Existing Approaches to Energy-Efficient CH Selection

Broadly, existing energy-efficient CH selection methods can be grouped into: (i) probabilistic rotation, (ii) residual energy-aware selection, (iii) location/distance aware and multi-criteria selection, and (iv) optimization/ metaheuristic and intelligent methods; many modern protocols combine elements from multiple groups [46], [47], [48], [49], [50], [51], [52] (Table 7).

Table 7. Comparison of CH selection families.

CH selection family	Core idea	Typical metrics	Strengths	Common drawbacks
Probabilistic rotation (e.g., LEACH baseline)	Nodes self-elect as CH with probability; rotate roles by rounds	Probability P, epoch/round counter	Very low overhead; fully distributed; scalable	May select low-energy nodes as CHs; uneven CH spatial distribution
Residual energy–aware	Bias CH choice toward higher remaining energy	Residual energy, energy rate/cost	Better energy balancing; longer lifetime	Requires energy estimation or reporting; added overhead in some designs
Distance/multi-criteria	Jointly optimize energy and communication cost	Energy, distance to sink/CH, density, cost	More uniform clusters; reduced comms energy	Requires parameter tuning; may need localization or more state exchange
Metaheuristic, intelligent	Solve CH selection as optimization problem	Multi objective fitness (energy, distance, load, etc.)	Near optimal CH sets; robust under complex objectives	Higher computation; longer convergence; may require global knowledge

A foundational approach is probabilistic rotation, in which each node becomes a CH with a predefined probability to ensure that the CH burden is distributed over time. The appeal of this strategy lies in its simplicity: it is fully distributed, incurs minimal overhead, and requires almost no state information, making it suitable for large-scale or resource-limited networks. Its primary drawback is randomness—CHs may be spatially uneven or may include nodes with low remaining energy, which can shorten the stable operating period and trigger early node failures [49].

To address these shortcomings, many protocols incorporate residual energy into the CH selection process. By preferentially selecting higher energy nodes as CHs, these schemes mitigate premature depletion of weaker nodes and achieve more balanced energy consumption. However, this improvement typically requires periodic reporting of residual energy or estimation mechanisms, which can introduce non-negligible overhead. In centralized variants (e.g., LEACH C type protocols), nodes send energy and/or location information to a base station, enabling more optimal CH layouts but at the cost of increased control plane energy consumption [49], [50].

A third family relies on distance-aware or multi-criteria selection, where CHs are chosen based on geometric, topological, or link quality considerations, often in combination with residual energy. By selecting CHs that minimize intra cluster distances or reduce CH to sink transmission cost, these methods produce more uniformly sized clusters and reduce communication energy. Multi-criteria approaches frequently use fuzzy logic to manage competing objectives—such as high energy, short distance, good link quality, and appropriate node density—without relying on brittle linear weightings that can be difficult to tune across heterogeneous deployments. This flexibility comes at the cost of increased complexity and a need for more state information (e.g., localization, neighbor tables) [49], [51], [52], [53].

More recent work treats CH selection as a multi-objective optimization problem, leveraging evolutionary and swarm intelligence algorithms (e.g., PSO variants, Grey Wolf Optimization, Harris Hawks Optimization) to identify near optimal CH sets under complex constraints. These metaheuristic approaches typically provide superior energy balancing, improved coverage, and extended lifetime compared to simpler heuristics. However, they may require greater computational resources, larger data exchanges, or global network knowledge—challenges for severely resource-constrained UASs or sensor nodes [51]. Overall, the Low Energy Adaptive Clustering Hierarchy (LEACH) protocol remains the foundational benchmark against which improved clustering strategies are compared. Its probabilistic rotation principle has inspired a broad spectrum of enhancements incorporating energy

awareness, geometry, multi-criteria reasoning, and intelligent optimization, each addressing specific limitations while introducing new tradeoffs.

6.2 The Essence of LEACH

LEACH is the is one of the earliest and most widely adopted hierarchical routing protocols for Wireless Sensor Network (WSNs) that introduced a self-organizing clustering mechanism with periodic CH rotation and in-cluster data aggregation, aiming to distribute energy consumption more evenly and thereby extend network lifetime. LEACH couples clustering with a time division multiple access (TDMA) based intra cluster medium access schedule and uses data fusion/aggregation at CHs to reduce the amount of information transmitted to the base station (sink) [46].

Key LEACH design principles:

- Randomized CH rotation for load balancing. LEACH's defining idea is that CH responsibility should rotate so that no subset of nodes is permanently burdened with energy-expensive long-range transmission and aggregation.
- Local coordination and scalable self-organization. Cluster formation is distributed and does not require global topology knowledge, supporting scalability.
- Data aggregation to reduce redundancy. By fusing data at CHs, LEACH reduces the number of bits delivered to the sink, directly lowering radio energy usage.
- Scheduled medium access via TDMA. TDMA scheduling within clusters allows non-CH nodes to turn off their radios outside their assigned slots (each node in a cluster is assigned one slot), minimizing idle listening and saving energy.

Classic LEACH assumes that CHs can transmit directly to the sink and that nodes are relatively homogeneous in terms of capability and initial energy. These assumptions can become restrictive in large-scale networks or irregular deployments where single-hop CH-to-sink communication is inefficient. Furthermore, because CH election is probabilistic and not inherently residual-energy aware, LEACH may select low-energy nodes or produce non-uniform spatial distributions of CHs, which can lead to uneven clusters and reduced network lifetime. These limitations motivated numerous variants, including centralized CH selection (LEACH-C), multi-hop extensions, and energy-aware threshold modifications [46], [47], [48], [49].

LEACH operates in rounds, each divided into a setup phase (CH election and cluster formation and) and a steady-state phase (data collection, aggregation, and forwarding).

In round r of the setup phase, each node independently decides whether to become a CH with a desired probability P, ensuring that approximately a fixed fraction of nodes becomes CHs each round. The standard LEACH threshold function selects node n as CH if [46]

$$\text{rand}(0, 1) < T(n) \tag{11}$$

where a threshold $T(n)$ is defined as

$$T(n) = \begin{cases} \frac{P}{1-P(r \mod 1/P)} & n \in G \\ 0 & \text{otherwise} \end{cases} \tag{12}$$

In Equation 12, G is the set of nodes that have not served as CHs during the previous epoch

$$\text{Epoch length} = 1/P \text{ rounds} \tag{13}$$

(The mod operator calculates the integer remainder of the division of r (dividend) by $1/P$ (divisor).)

Threshold 12 ensures that each node becomes a CH roughly once per epoch, preventing repeated selection of the same energy-critical nodes.

Elected CHs broadcast advertisement messages, non-CH nodes select CHs (often based on strongest received signal strength), and CHs assign TDMA slots to their members to avoid collisions and reduce idle listening.

Figures 11a and 11b show an example of CH selection and resulting clustering for a 100 node UAS swarm deployed in a 100 m × 100 m area with a target CH percentage of 0.05 at round index 7.

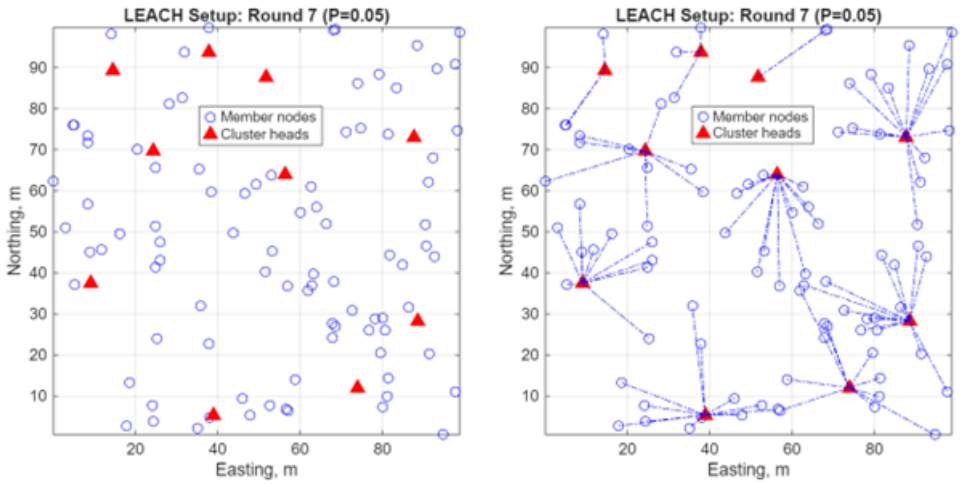

(a) (b)

Figure 11. Snapshot of CH assignment (a) and UAS clustering (b).

During the steady-state phase, member nodes transmit sensed data to the CH according to their TDMA slots. CHs aggregate or compress the received data to eliminate redundancy and then send the aggregated information directly through a swarm relay—typically a node located farthest from the jamming source—toward BS. This final transmission is energy intensive due to its long range, making CH selection a critical factor in determining network lifetime.

This operational structure provides

- Randomized CH rotation: preventing persistent energy hotspots
- Localized coordination: reducing control overhead
- Data aggregation: lowering overall data transmission volume
- Single-hop CH-to-BS communication: effective in small- and medium-scale deployments

Despite its effectiveness and simplicity, LEACH's assumptions—homogeneous energy, single-hop CH-to-sink communication, and probabilistic CH election—limit its suitability in many real-world scenarios. These constraints inspired a broad family of extensions and alternative clustering strategies (Figure 12 and Table 8), including centralized, energy-aware,

distance-aware, fuzzy logic-based, and metaheuristic optimization approaches, each aimed at addressing specific weaknesses of the baseline protocol.

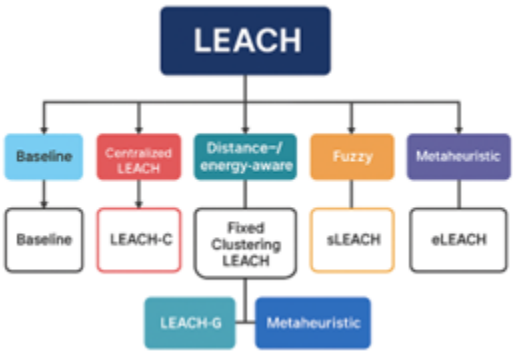

Figure 12. LEACH taxonomy diagram.

Table 8. Differences of some LEACH variants from the baseline LEACH and from alternative clustering schemes of CH selection family.

Protocol	Type	CH selection method	Advantages	Drawbacks
LEACH	Distributed	Probabilistic, random	Very low overhead, simple	Uneven clusters; low-energy CHs
LEACH C	Centralized	BS optimizes CHs using energy + location	Uniform clusters, better lifetime	Higher-control traffic; less scalable
LEACH F	Centralized	Clusters fixed, CH role rotates	Very low overhead after setup	Not adaptive to topology changes
sLEACH	Distributed or Hybrid	Favors solar-powered nodes	Great lifetime improvements with solar	Environment dependent
eLEACH	Distributed	Residual energy enhanced probability	More balanced energy usage	More overhead than LEACH
Alternative clustering	Varies	Energy aware, distance aware, fuzzy, metaheuristic	Best performance; adaptive	Higher complexity/overhead

6.3 Relationship Between Round, Epoch, and Time

A round is the fundamental operational time unit in LEACH. As described in the previous section, each round consists of seven main phases:

1. Setup phase
2. CH election
3. Cluster formation through ADV, JOIN, and TDMA control messages
4. Steady-state phase (much longer than setup)
5. TDMA schedule execution operation
6. The CH aggregates or compresses received data
7. The CH transmits the aggregated packet to BS

Importantly, LEACH does not prescribe a fixed duration for a round. Instead, the round length is fully determined by the system designer and depends on factors such as the sensing rate and application reporting requirements [46].

An epoch is a logical interval used to ensure fair CH rotation. Under LEACH's threshold mechanism, each node becomes a CH once per epoch on average. Using Equation 13 with a desired CH probability of $P = 0.05$, one epoch contains 20 rounds. This ensures that all nodes have equal probability of serving as a CH within each epoch, thereby promoting balanced energy consumption.

How do rounds relate to actual time? The real duration of a round depends on system-level timing parameters, including

- Sensor sampling rate
- Required application reporting frequency
- TDMA schedule length
- Radio transmission data rate
- Setup phase message timings

For example, If the TDMA frame is 1 second and there are 30 slots, then steady-state is 30 s. Adding a setup stage of a few hundred ms, yields 31 seconds round duration. If sampled once per minute, one round lasts about 60 seconds.

For the higher rate sensing, (e.g., 10 Hz or 0.1 s per sample), one round becomes approximately 0.1 s (though LEACH is not well suited for high-rate applications and such rates are not expected in UAS swarm operations).

Now, consider a simple example. If

- $p = 0.05 \Rightarrow$ epoch = 20 rounds
- duration of a round = 10 seconds
- 20 rounds = 200 seconds

then

- Epoch time $\approx$ 200 seconds

Table 9 puts everything all together while Figures 13 and 14 visualize a representative example.

Table 9. Relationship between round, epoch, and time.

Concept	**Definition**	**Related to time?**	**Typical value**
Round	One full cycle: setup + steady-state	Yes, chosen by designer	Application-dependent (seconds to minutes)
Epoch	Number of rounds required for each node to become CH exactly once	No, purely logical	1/p, e.g., 20
Actual time	Total runtime of system	Depends on duration of each round	Rounds × (duration of 1 round)

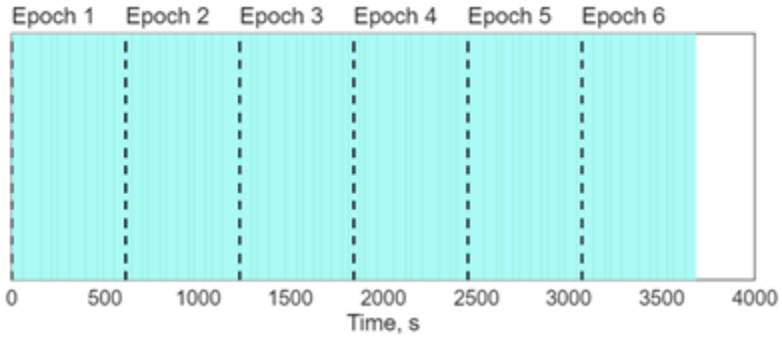

Figure 13. LEACH Rounds Timeline (120 rounds, epoch approx. 20 rounds).

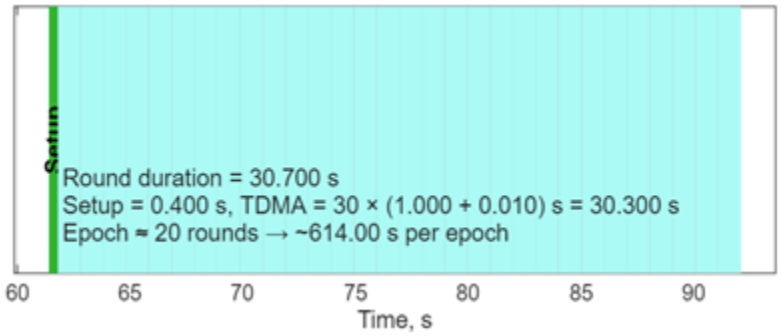

Figure 14. Round 3 Breakdown (Setup + 30 TDMA slots).

6.4 Radio Energy Dissipation Model

Let us modify a threshold $T(n)$ by multiplying it with the ratio of the residual energy at UAS n to initial energy, E_{res}/E_{int} , to balance total energy consumption across the entire swarm, not only to promote high-energy nodes as in eLEACH protocol (Table 8):

$$T(n) = \begin{cases} \frac{E_{res}}{E_{int}} \frac{P}{1-P(r \mod 1/P)} k_{opt} & n \in G \\ 0 & \text{otherwise} \end{cases} \tag{14}$$

As a result, UAS swarm nodes are prevented from being overburdened when their energy is low, thereby extending the operational lifetime of the entire network. Equation 14 also integrates the optimal number of clusters k_{opt} to be defined later.

To accurately estimate energy consumption, let us adopt the classical first-order radio energy dissipation model. In this model, the transmitter expends energy on both radio electronics and the power amplifier, while the receiver consumes energy only for electronic circuitry. Depending on the transmission distance, either the free-space path-loss model (d^2) or the multipath fading model (d^4) is applied.

For a message of l bits transmitted over distance d, the energy consumed is

$$E_{Tx}(l,d) = \begin{cases} lE_{elec} + l\epsilon_{fs}d^2 & d < d_0 \\ lE_{elec} + l\epsilon_{mp}d^4 & d \geq d_0 \end{cases} \tag{15}$$

where $d_0 = \epsilon\sqrt{\epsilon_s / \epsilon_{mp}}$ is the threshold distance separating the two channel models.

Having Equation 15, the optimal number of clusters in Equation 14 can be defined as [54]:

$$k_{opt} = \frac{\sqrt{n}}{\sqrt{2\pi}} d_0 \left(\frac{d_{toBS}}{M} \right)^2 \tag{16}$$

In Equation 16, $M \times M$ is the size of the deployment region, and d_{toBS} is the average distance from the UAS swarm to the BS. This ensures that the resulting cluster configuration minimizes overall energy dissipation.

The energy to receive an l-bit packet is given by

$$E_{Rx}(l) = lE_{elec} \tag{17}$$

This model enables the evaluation of transmission and reception costs under varying network conditions.

To demonstrate random CH selecting effect on communication energy consumption, let us keep considering the same network as illustrated in Figure 11. Each node starts with 0.5 J of initial energy and is considered dead when its energy falls below the energy threshold required for data transmission. Other parameters used in simulations (Table 10) will be consistent with the previous efforts [46], [47], [48], [49]. Following these efforts, the optimal number of clusters (k_{opt}) is chosen between 1 and 6. As opposed to the stationary network considered in the previous research, this research is based on the agile swarm operations when all UAS are constantly moving, pursuing several objectives, described in the next section.

Table 10. Summary of the parameters used in simulation experiments.

Parameter	**Value**
Field size ($M \times M$)	100 m × 100 m
Location of BS (Base Station)	75 m < d_{toBS} < 185 m
Number of nodes (N)	100 nodes
CH probability	0.1
Initial energy of sensor node	0.5 J
E_{Tx} and E_{Rx} (E_{elec})	50 nJ/bit
Free space coefficient (ϵ_{fs})	10 pJ/bit/m^2
Multipath fading coefficient (ϵ_{mp})	0.0013 pJ/bit/m^4
Energy for aggregation (EDA)	5 nJ/bit/signal
Data packet size (l)	4,000 bits

6.5 Decentralized UAS Swarm Dynamics

The previous work by the authors [54] introduced a decentralized, behavior-based outer loop controller that allows each UAS in the swarm to autonomously compute its desired velocity setpoint based solely on locally available information. The controller was designed to accommodate multiple swarm behaviors—area search, network maintenance, or combinations thereof—and map operator selectable behavioral primitives to a unified mathematical structure. A key objective was enabling scalable, reactive, and communication efficient swarm behavior without relying on a central coordinator.

At each control cycle, every UAS evaluates a set of four input vectors that encode the local spatial configuration of the swarm and the agent's search progress history. These inputs are:

1. Direction to the closest neighbor
2. Direction to the second closest neighbor
3. Direction to the third closest neighbor
4. Direction to the least visited neighboring grid cell

The first three drivers capture the spatial relationship to nearby agents and enable cohesion, dispersion, and formation-keeping behaviors. The fourth driver encourages exploration by biasing motion toward underexplored regions of the environment. Importantly, during field tests each UAS maintained its own visitation histogram without inter agent synchronization, reducing communication overhead and eliminating the need for consistent shared maps.

Each driver is expressed as a 2D vector

$$F_i \in R^2, i = 1, ..., 4, \tag{18}$$

directed from the agent's current position either toward a neighboring UAS or toward the center of a selected low-coverage grid cell. The corresponding distances

$$d_i = ||F_i|| \tag{19}$$

serve as arguments to the controller's parametric weighting functions.

Rather than switching between behaviors or defining hard rules, the controller blends the four directional drivers into a single desired velocity vector. This blending is achieved through parametric weights that encode attraction, repulsion, and distance-keeping effects. The final velocity setpoint is

$$v_{SP} = \frac{1}{4} \sum_{i=1}^{4} w_i(d_i) \frac{F_i}{||F_i||} \tag{20}$$

The weight for each input is the sum of two components, as defined as

$$w_i(d_i) = a_i(d_i) + g_i(d_i) \tag{21}$$

The component $a_i(d_i)$ in Equation 21 modulates long-range attraction or repulsion using a smooth sigmoid centered at distance c_i

$$a_i(d_i) = k_i \left(\frac{2}{1 + e^{(d_i - c_i)/\epsilon_i}} - 1 \right) \tag{22}$$

This term smoothly transitions between $+k_i$ (attraction) and $-k_i$ (repulsion), shaping global tendencies such as spreading out for area search or clustering for network maintenance. The second term in 21 promotes stabilization around a preferred distance c_i:

$$g_i(d_i) = 2t_i(d_i - c_i)e^{(d_i - c_i)^2/\epsilon_i^2} \tag{23}$$

This "gravity well" function is effectively the derivative of a Gaussian centered at c_i, generating a restoring force that maintains inter agent separation—for example, holding approximately 30 m spacing during network maintenance missions.

By appropriately selecting the parameter vectors

$$k, t, c, \epsilon, \tag{24}$$

the same controller can express qualitatively different swarm behaviors. Ref. [54] provides the parameter sets used to realize pure search (exploration), pure network maintenance, or a combination of the two.

The outer loop controller computes the planar velocity setpoint v_{SP}, which is transmitted to the flight controller's inner loop onboard autopilot. The autopilot adjusts the UAS's accelerations to minimize the error $||v - v_{SP}||$, closing the low-level feedback loop. This cascaded architecture allows

- the outer loop to focus on swarm level interactions
- the inner loop to handle vehicle dynamics and stabilization, and
- the agents to maintain decentralized operation even with intermittent communications

Figure 15 shows an example of a multi-function swarm UAS simulation exhibiting different behaviors. Specifically, controllers in Figure 15a focus on exploration, in Figure 15b on network maintenance, and in Figure 15c on a combination of the two objectives.

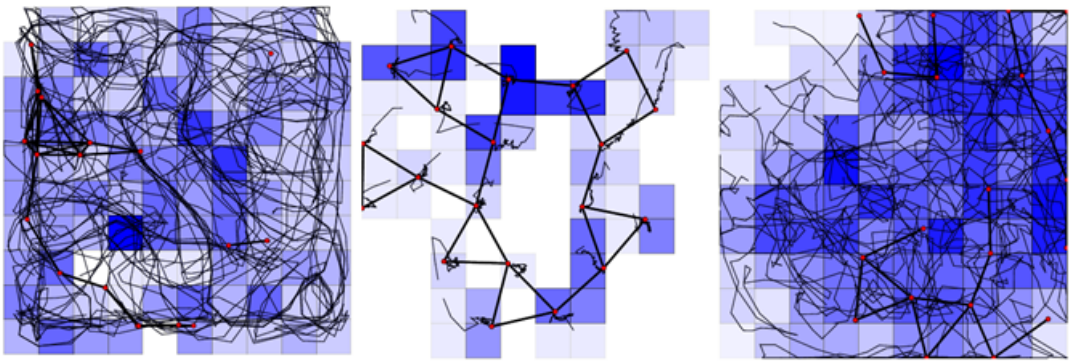

Figure 15. Three different controllers for a multi-function swarm.

A central advantage of the algorithm is that all computations are performed locally on each UAS's companion computer, using only neighbor telemetry received via the swarm network. As a consequence,

- The swarm naturally scales to additional agents without increasing central load.
- Loss of link or temporary packet dropouts do not halt the swarm—agents continue operation based on last known observations.
- Collision avoidance emerges from the repulsive components of the weighted inputs, without requiring global coordination.

This reactive, rule-based design mirrors classical biologically inspired swarm systems while supporting operational tasks such as search and rescue, communication relay formation keeping, and mixed-mode behaviors.

6.6 Mesh-Network Evaluation Metrics

In LEACH and most wireless sensor network (WSN) protocols, network performance and lifetime are assessed using a set of well-established evaluation metrics. These metrics enable comparison of energy efficiency, stability, coverage, data-delivery performance, and protocol overhead.

1. Lifetime metrics – These metrics characterize the longevity and stability of the network:

- First node dies (FND): number of rounds until the first node depletes its energy
- Half nodes die (HND): number of rounds until 50
- Last node dies (LND): total number of rounds until the final node dies
- Stability period: interval between deployment and the point at which the first node dies

2. Energy-related metrics – These metrics assess energy usage and balance:
   - Total energy consumption per round: amount of energy consumed during each iteration
   - Remaining energy vs. rounds: tracks energy depletion trends and load-balancing effectiveness
   - Average energy consumption per node: useful for comparing cluster head (CH) vs. non CH nodes
3. Data delivery metrics – These quantify communication effectiveness:
   - Number of packets sent to BS: measures end-to-end throughput
   - Number of packets sent to cluster heads: indicates quality of intra cluster communication
   - Total Data delivered: total packets successfully received at the BS
4. Cluster-related metrics – These evaluate clustering performance and fairness:
   - Number of CHs per round: LEACH attempts to maintain 5
   - Cluster formation efficiency: consistency and spatial fairness of cluster formation
   - CH rotation frequency: indicates how well the protocol distributes energy load over time
5. Coverage and connectivity metrics – These assess network usability and sensing performance:
   - Sensing coverage over time: percentage of monitored area covered by active sensors
   - Network connectivity: ability of nodes to route data to a CH or the BS
   - Functional lifetime (FL): the first round in which sensing coverage drops below the required coverage threshold, or network connectivity falls below the connec-tivity threshold. FL emphasizes that a network may remain partially powered (i.e., some nodes still have residual energy), yet be operationally ineffective once it can no longer maintain adequate sensing or communication performance.

6. Delay and latency metrics – Relevant for comparing LEACH with time-sensitive protocols:
    - Communication delay: time for a packet to reach the BS
    - End-to-end latency: important when evaluating LEACH vs. other protocols
7. Overhead metrics – These capture communication and control burden:
    - Control Overhead: Messages and energy spent on advertisements, cluster formation, and synchronization
    - Overhead per round: useful for comparing LEACH with its variants (LEACH C, LEACH M, etc.)

Table 11 provides a summary of these metrics.

Table 11. WSN protocol metrics.

Category	**Metric**	**Purpose**
Lifetime	FND, HND, LND, stability period	Evaluate longevity
Energy	Total energy, avg. energy, remaining energy	Measure efficiency
Data Delivery	Packets to BS/CH	Assess throughput
Cluster	Metrics CH count, cluster balance	Check clustering quality
Coverage	Area coverage, connectivity	Assess usefulness of network
Delay	Latency, end-to-end delay	Evaluate performance time
Overhead	Control overhead	Compare protocol efficiency

For the practical application considered here, the developed algorithms are evaluated using two primary performance indicators:

1. Network lifetime, defined as the number of rounds completed when the first node exhausts its energy. Maximizing the time to FND directly increases the operational duration of the system
2. Collected data volume, which represents the amount of data successfully delivered to the base station, reflecting the system's data collection effectiveness

From a system-level perspective, an additional desirable property is a short death window, meaning that once nodes begin to fail, all nodes die within a relatively narrow time interval. This ensures that the network remains fully functional for as long as possible before complete degradation. This criterion is consistent with prior work [46].

6.7 Computer Simulation

This subsection presents the results of the integrated simulation environment that incorporates all algorithms and mechanisms described earlier in this section, including CH election, member–CH association, multi-hop CH to BS routing, energy consumption modeling, dynamic swarm behavior, and coverage and connectivity assessment. In addition to the parameters defined in Table 10, Table 12 summarizes the remaining simulation parameters employed in the study. Along with supporting the homogeneous LEACH protocol—where all swarm nodes begin with equal initial energy—the developed simulation framework also accommodates heterogeneous network configurations in which certain nodes (e.g., advanced, super, or gateway nodes) possess higher energy reserves or enhanced capabilities.

Table 12. Simulation parameters.

Simulation parameter	**Value**
Base station coordinates	[175,50] m
Sensing radius	10 m
Communication radius member→BS	30 m
Communication radius CH→CH for multi-hop layer	60 m
Communication radius CH→BS	120 m
Free space/multi-path crossover distance: d_0	87.71 m
Min coverage ratio required	0.90
Min fraction of alive nodes connected to BS	0.95
Fixed setup duration	0.40 s
Fixed TDMA slots	30
Fixed slot	1.00 s
Guard per slot	0.01 s

Specifically, the stable election protocol (SEP) features normal nodes with initial energy E0 and advanced nodes with initial energy E_0 $(1 + \alpha)$. Their respective CH election probabilities are

$$P_{normal} = \frac{P_{opt}}{1 + \alpha m} \quad \text{and} \quad P_{advanced} = \frac{P_{opt}(1 + \alpha)}{1 + \alpha m} \tag{25}$$

where m denotes the fraction of advanced nodes and α represents the additional energy factor. In the simulation, the parameters m and α are set to 0.1 and 1.0, respectively. Because advanced nodes start with higher energy, they shoulder a greater portion of the commu-

nication load, resulting in later node deaths and an extended stability period compared to homogeneous LEACH. The distributed energy-efficient protocol (DEEP) further generalizes heterogeneity by supporting multi level energy distributions. In DEEP, the CH election probability for each node i is proportional to its residual energy E_i, the initial heterogeneity level, and the average network energy $\bar{E}$:

$$p_i = p_{opt} \frac{E_i}{\bar{E}} \tag{26}$$

This approach yields more balanced energy consumption among nodes, enhances network longevity compared to LEACH and SEP, and ensures dynamic, energy-aware CH selection as the network evolves. In addition to traditional single-hop communication—where each CH transmits directly to BS—the simulation framework also supports multi-hop CH-to-BS routing. In this mode, CHs forward data through other CHs rather than transmitting over long distances directly to the BS. This significantly reduces the energy burden on CHs located far from the BS, distributes the communication load across the CH hierarchy, and further prolongs the overall network lifetime, particularly in large-scale or unevenly distributed deployments.

Figure 16 shows the number of alive nodes throughout the full 5,000-round experiment, while Figure 17 displays the cumulative simulation time corresponding to these rounds (1,912.7 seconds, derived per round from bitrate and frames and varying per found with cluster sizes rather than direct timing, fixed per round). The upper x axis in Figure 16 and the subsequent figures maps the round index to the corresponding cumulative simulation time. Figure 18 presents the total residual energy remaining in the UAS swarm as the simulation progresses, and Figure 19 provides a per node view of residual energy over time, illustrating heterogeneity in energy consumption across individual UAS due to their differing roles (member vs. CH, routing load, etc.).

Figure 20 shows the per round data packets successfully forwarded to the BS, along with the aggregate throughput (dual Y axis) accumulated via the multi-hop CH layer routing process.

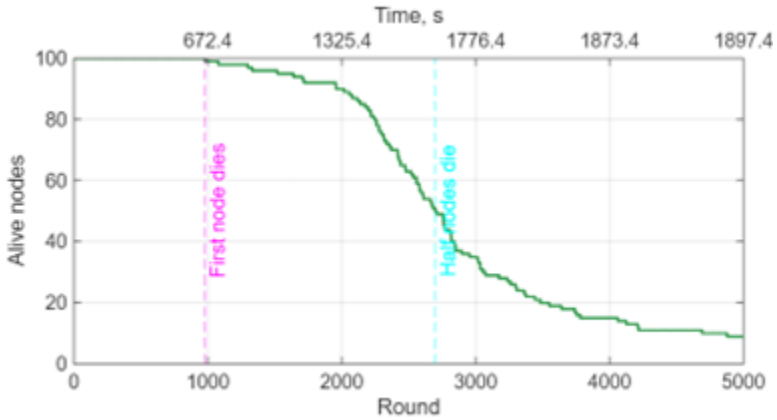

Figure 16. Alive nodes vs. rounds (LEACH, multi-hop CH → BS).

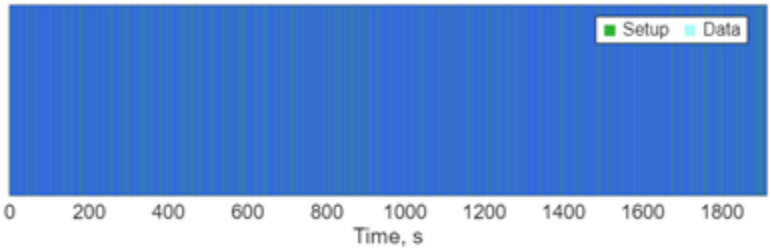

Figure 17. Per-round timeline (setup vs. data).

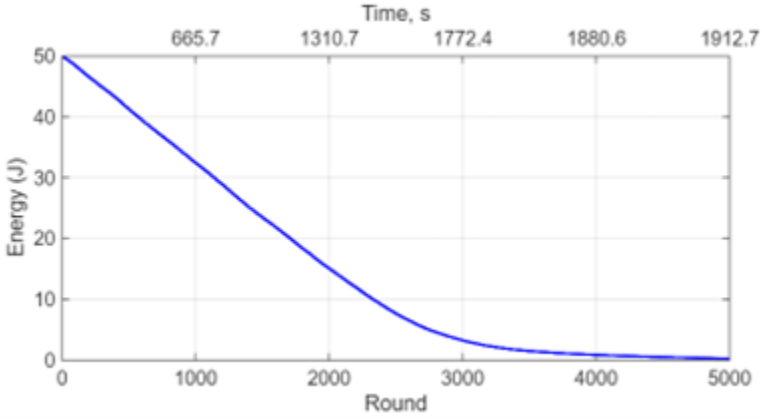

Figure 18. Total residual energy.

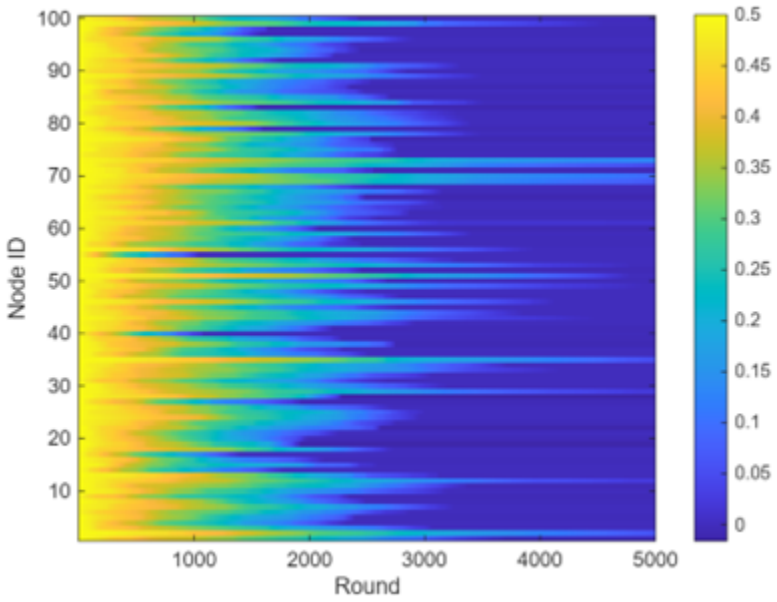

Figure 19. Residual energy per node over time (J).

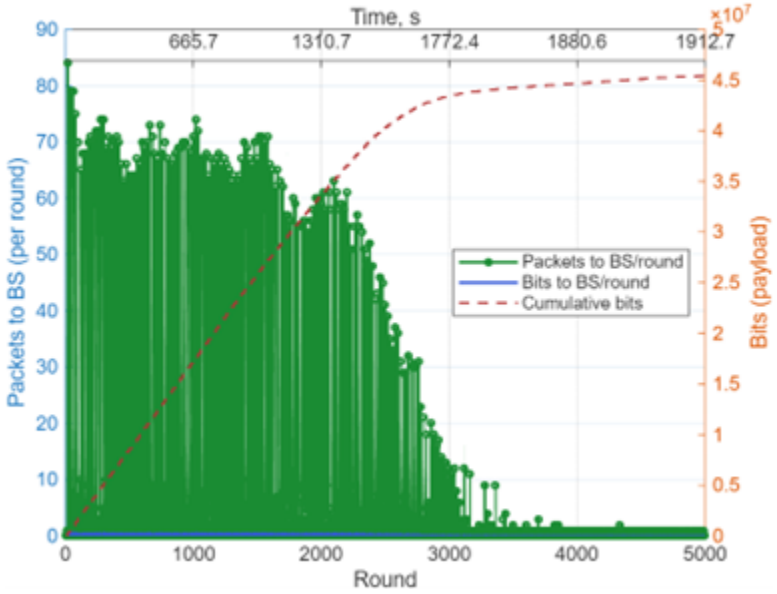

Figure 20. Aggregate throughput to BS.

At each round, the simulator evaluates all three coverage and connectivity metrics:

- Coverage, the fraction of the field area covered by at least one alive node within the sensing radius R_s. This is computed over a raster grid spanning the field.
- Connectivity, the fraction of alive nodes that possess a valid communication route to the BS. A node is considered connected only if:
  1. It is a CH located within $R_{c,BS}$ of the BS, or
  2. It is a member of a CH within $R_{c,member}$, and that CH itself is connected to the BS (either directly or via multi-hop CH links).
- FL, defined as the first round in which either coverage drops below the required coverage threshold, or connectivity drops below the connectivity threshold.

Note that classical LEACH, with its implicit assumption of high-power long-range CH → BS transmission, can achieve long BS reachability distances. Setting $R_{c,BS}$ large in the geometric model approximates this behavior and shifts FL sensitivity toward coverage rather than BS reachability.

Figures 21 and 22 show the time history of these two metrics. The FL reported in Figures 16, 21, and 22 is evaluated based on these thresholds.

Figure 23 shows the spatial layout of all UAS at the end of the simulation, including the assumed BS (lead node) location. Node colors indicate the fraction of residual energy remaining, providing a spatial perspective on energy-depletion patterns across the field.

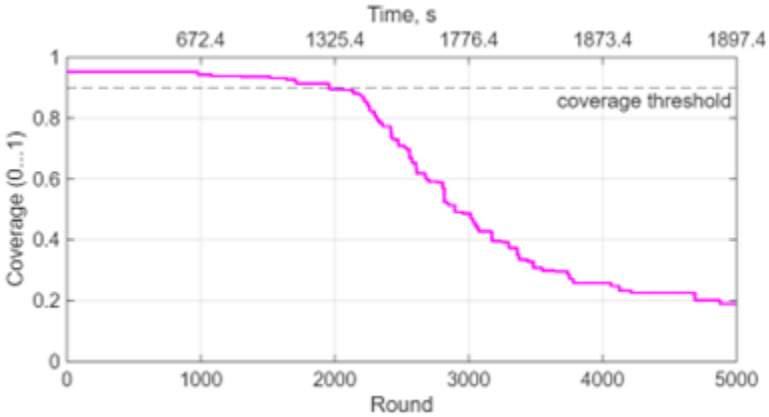

Figure 21. Coverage ratio (area).

Output parameter	Value
First Node dies (FND)	1,039
Half of nodes die (HND)	2,748
Last node dies (LND)	n/a (i.e., not all nodes died by 5,000 rounds)
Average CHs per round	3.13
Average packets delivered to BS per round (all CHs)	3.13
Total packets forwarded to BS	11,350
Total bits forwarded to BS	45,400,000 bits
Average effective throughput	2.27 packets/round, 9080 bits/round

Figure 22. Connectivity to BS (multi-hop CH layer).

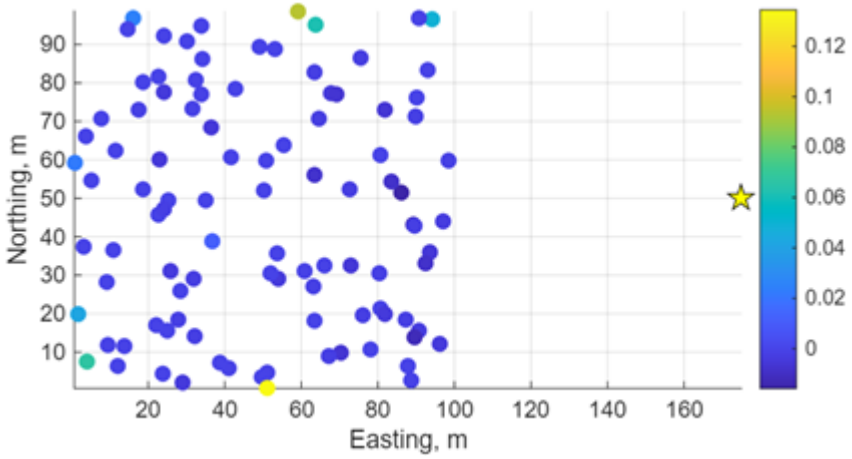

Figure 23. Residual energy by node (final round).

Table 13 summarizes the key observations from the 5,000-round LEACH-based simulation with multi-hop CH → BS routing and dynamic node states.

Table 13. Key observations.

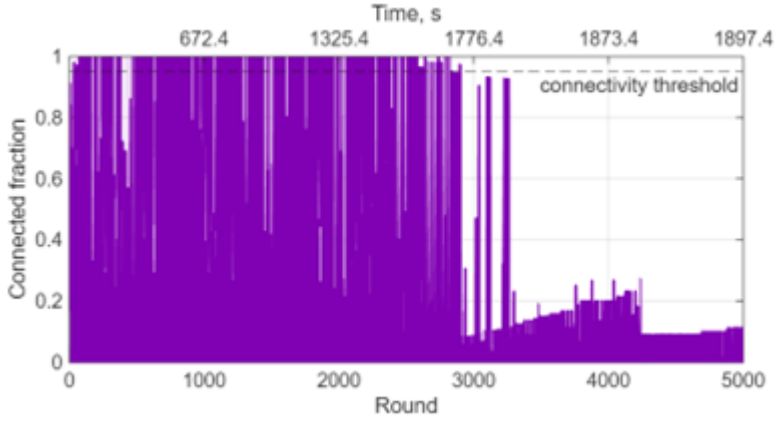

7 Flight-Testing Trials

A series of unforeseen circumstances—including significant faculty losses following the deferred resignation program, travel restrictions that limited operations to the nearest test range, two furlough periods, substantial budget reductions that eliminated test-range support, and procurement delays caused by tariffs—collectively prevented the execution of the full-scale experimental campaign originally planned to validate the developed algorithms. The authors hope that NPS UAS testing capabilities will be fully restored in the future, enabling continued advancement, characterization, and evaluation of mesh-networking algorithms to ensure UAS swarming superiority. The following subsections summarize several limited experimental efforts conducted during this project to test and verify the algorithms developed in Section 6.

7.1 Linear Network Testing with MR UAS

This subsection describes a data-collection effort conducted during the Joint Interagency Field Experimentation (JIFX) 25-3 event, hosted by the NPS Information Sciences Department from May 12–16, 2025. The primary objective was to evaluate the performance of a small multi-vehicle surrogate UAS equipped with MANET capabilities. Operation of this system provided an opportunity to gather empirical data on communication-relay effectiveness within a linear UAS network topology.

Figure 24 shows the Group 1 GreenSight Dreamer UAS platforms used in the field trials. Each of the six aircraft (two of which are shown in Figure 24a) was integrated with Rajant mesh radios configured to operate across two distinct frequency bands (Figure 24b). To

support this dual-band capability, the platforms employed two types of omnidirectional antennas, providing redundancy and ensuring robust connectivity under dynamic network conditions. This configuration was essential for maintaining resilient communication links during complex swarm-operation scenarios, including those simulating contested or degraded environments.

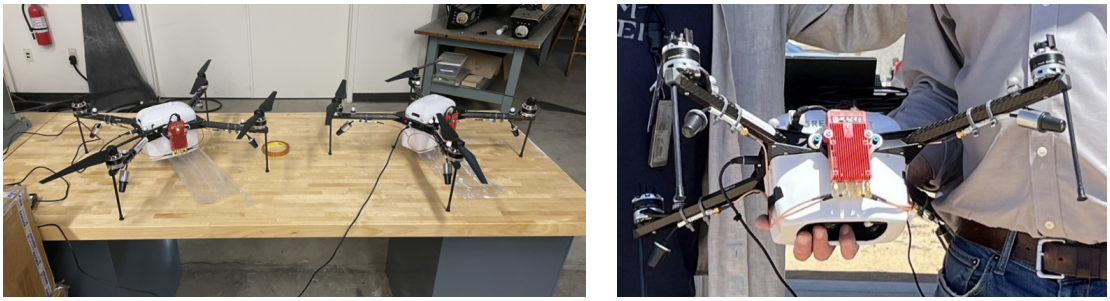

(a) (b)

Figure 24. GreenSight Dreamer UAS integrated with Rajant radios.

Figure 25 depicts the slant range—defined as the distance between the UAS and the ground control station (GCS)—over time during a representative single-vehicle sortie at JIFX 25-3. In this flight, the UAS ascended to its operating altitude, traveled to a waypoint 800 m away while maintaining constant altitude, then returned to the launch site, descended, and landed.

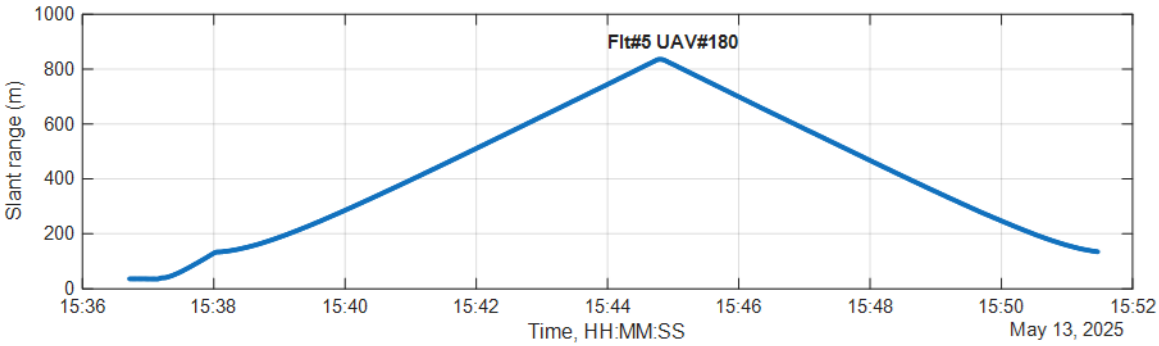

Figure 25. Slant range over time.

Figure 26 shows network latency, a metric representative of signal strength and link quality, as a function of slant range for the same flight. Latency was calculated by comparing the timestamps in MAVLink *SYSTEM_TIME* messages—taken from the UAS autopilot system clock at message generation—with the GCS system clock timestamp at message receipt.

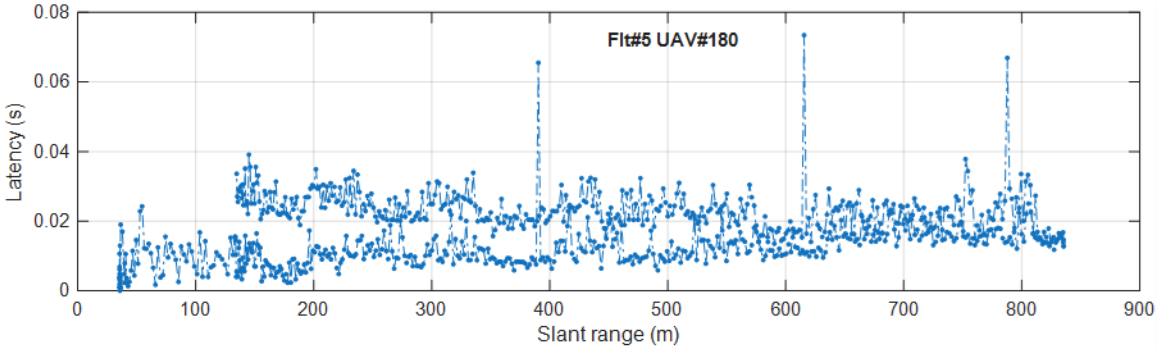

Figure 26. Latency versus slant range.

As shown in Figure 26, network latency remained relatively constant throughout the flight, indicating that the increasing distance between the UAS and GCS did not significantly affect network integrity.

7.2 UAS Swarming

The decentralized UAS-swarm dynamics described in Section 6 were fully implemented on a twenty-vehicle swarm using DX2 radios and validated through multiple field experiments (Figure 27). However, these demonstrations relied on 3DR-manufactured platforms that are no longer in production, limiting the ability to replicate the experimental configuration. Future experimentation campaigns will therefore transition to the Dreamer platforms described in the previous subsection.

(a) (b)

Figure 27. NPS UAS Swarm (a) and its operation (b).

7.3 Data Collection with a Fixed-Wing UAS

To estimate the volume and type of information expected to be gathered and preprocessed onboard each UAS, several platforms were used in recent data collection experiments.

The Freefly Systems “Astro” (Figure 28a) is a U.S.-manufactured commercial UAS designed for industrial applications, offering long-endurance, high-stabilization performance, and payload support for precision mapping and inspection—including thermal sensors for fire service operations. Several flights were conducted on February 27, 2026, at the Monterey Bay test range near La Selva Beach, CA, to collect electro optical (EO) sensor data for subsequent processing. Figure 28b shows faculty and students from the Electrical and Computer Engineering Department trained to operate this platform.

(a)

(b)

Figure 28. Freefly Astro with an integrated EO sensor payload (a) and the operating flight team (b).

Additional data-collection trials were performed using the Trinity Pro UAS, a recently acquired fixed-wing VTOL platform capable of carrying multiple sensor types. These trials occurred during two experimentation campaigns in January and February 2025. Figure 29 illustrates the aircraft transitioning from vertical takeoff with all three motors pointed upward (Figure 29a) to forward flight with the motors rotated horizontally (Figure 29b).

(a)

(b)

Figure 29. Trinity Pro vertical takeoff (a) and transition to horizontal flight (b).

Figures 30a and 30b depict representative flight profiles—one over land and one over the shoreline—flown during these trials.

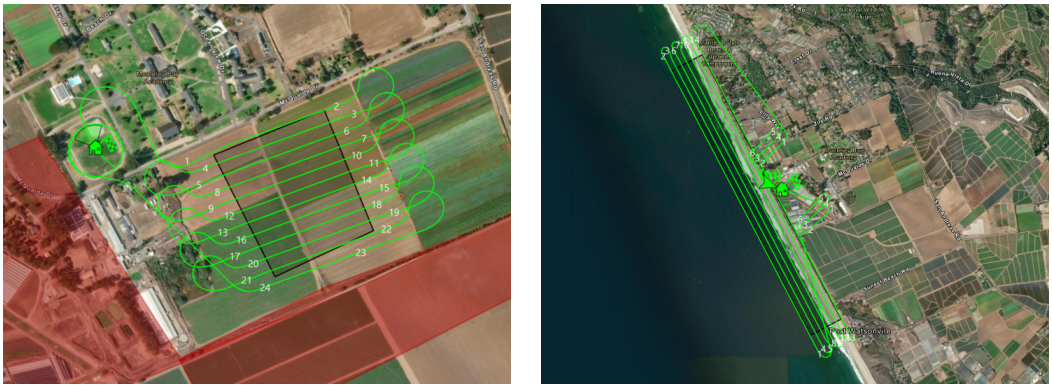

(a) (b)

Figure 30. Trinity Pro flight missions conducted over land (a) and over shoreline (b).

Although the EO sensor malfunctioned during these missions, lidar data was successfully collected and post-processed. Resulting 3D point-cloud models for both flight profiles are shown in Figures 31 and 32. These datasets will be further analyzed to enable automated detection of specific objects of interest.

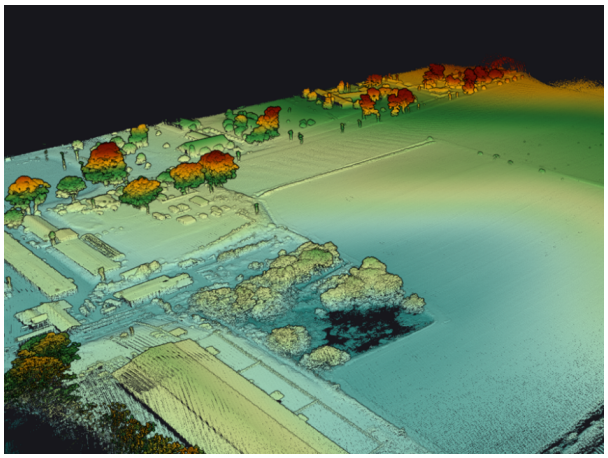

Figure 31. Example 3D point cloud model generated from over-land imagery.

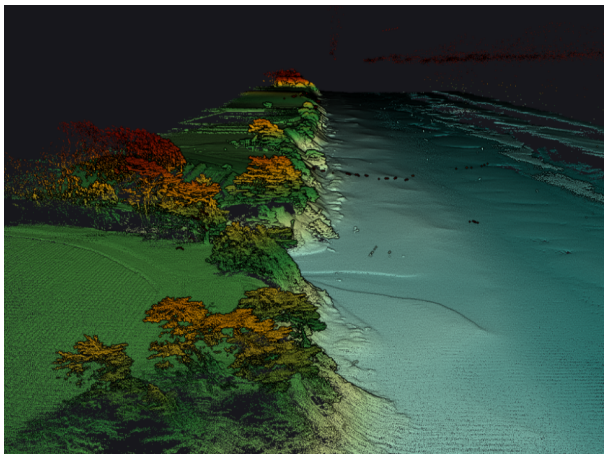

Figure 32. Example 3D point cloud model generated from over-shoreline imagery.

THIS PAGE INTENTIONALLY LEFT BLANK

8 Conclusion

This project explored the feasibility and operational potential of mesh-networked UAS to support targeting and data relay operations within contested, GPS-denied environments. Through a combination of analytical modeling, system architecture development, simulation, and flight testing, several overarching findings emerge.

First, linear and mesh-networking architectures provide complementary capabilities. Linear UAS chains can extend communication range between remote sensors and decision nodes but are highly sensitive to energy constraints, transit time budgets, and geometric placement. Mesh networks, by contrast, can dynamically reconfigure, provide multi-path routing, and maintain partial functionality under attrition—but their effectiveness depends on clustering strategies, swarm dynamics, and distributed sensing performance.

Second, energy-aware clustering is critical. LEACH and its variants offer a principled mechanism to balance communication load and prolong network lifetime. However, classical LEACH assumptions—static nodes, uniform spatial distribution, and single-hop CH→BS links—do not hold for highly dynamic, mobile UAS swarms. The preliminary results show that even with carefully tuned CH probability, the functional lifetime may collapse to a single round when coverage and connectivity thresholds are strict. This underscores the need for adaptive, geometry aware, and residual energy driven clustering tailored to mobile UAS networks.

Third, communication range and topology strongly govern feasibility. MANET radios such as the Rajant DX2 provide robust connectivity but do not dramatically increase the mesh's maximum viable geometry. Member→CH, CH→CH, and CH→BS radii remain the principal limiting factors determining cluster viability and end-to-end connectivity.

Fourth, flight testing validated core assumptions. Experiments involving Dreamer MR UAS and Trinity Pro FW UAS demonstrated that (i) MANET radios maintain stable latency across a broad range of slant ranges, (ii) decentralized swarm-control algorithms function under realistic telemetry dropouts, and (iii) multimodal sensing (EO, LiDAR) can produce high-quality spatial datasets for future autonomy and mapping algorithms.

Finally, this research highlighted that mesh-enabled targeting is as much a systems integration and operational architecture challenge as a networking problem. Achieving resilient kill web performance demands unified progress across communications, autonomy, sensing, energy-aware routing, and fielded platforms.

Overall, this research provides a rigorous foundation for future operational experimentation and identifies several pathways for maturing mesh networked UAS technologies to support naval and joint warfighting concepts in A2/AD and DDIL environments.

9 Future Work

The work completed in this project opens multiple promising research directions across modeling, autonomy, sensing, communications, and field experimentation. Future efforts will prioritize the following areas:

Simulation environments should be scaled to reflect operationally relevant mesh-network sizes. Such simulations must account for realistic terrain occlusion, atmospheric-propagation effects, and the presence of dynamic adversary jamming to support meaningful performance assessment.

Future research could incorporate expanded field testing and broader data collection. This includes conducting multi-UAS, multi-frequency flight experiments designed to capture interference effects, assess multi-hop MANET performance under motion, and quantify packet loss, latency, and path diversity under realistic conditions. Such experiments should also observe real-time cluster formation within a dynamically moving swarm. Beyond airborne systems, hybrid networks that integrate UAS, surface vehicles, and ground nodes should be evaluated to replicate operational maritime and littoral kill-web environments more faithfully.

Another important direction involves advancing adaptive and geometry-aware clustering. New clustering algorithms should incorporate real-time geometric relationships among nodes, residual energy levels, link-quality estimates, and sensing-coverage priorities. To mitigate the inherent randomness of LEACH-based protocols, alternative cluster-head selection mechanisms—such as fuzzy-logic approaches or reinforcement-learning-driven policies—should be investigated for more stable and predictable network behavior.

Distributed sensing and cooperative targeting capabilities should be explored further. Swarm-level algorithms can be extended to fuse EO/IR cues, LiDAR-derived terrain information, RF-based ranging, and cooperative target-tracking estimates into a more cohesive situational picture. In parallel, robust target handoff mechanisms should be developed to ensure continuity of tracking across UAS, especially under DDIL communications conditions.

Integrating these technical advances with Navy concepts of operations and emerging kill-web architectures is essential. Research should evaluate how mesh-networked UAS can support stand-in forces, amphibious missions, long-range maritime reconnaissance, and distributed fires—particularly with respect to rapid kill-chain closure. Defining interface

and protocol requirements for connecting mesh-enabled UAS with NIFC-CA, JADC2, and similar frameworks will ensure alignment with broader naval command-and-control systems.

Finally, future efforts should emphasize operational experimentation and the development of effective human–machine-team interfaces. This includes designing supervisory-control tools capable of managing large swarms while minimizing cognitive burden on operators. Ethical, doctrinal, and operational considerations associated with highly autonomous, mesh-enabled targeting will also require careful study to ensure responsible integration into fleet operations.

List of References

[1] "Drone Defense for your Airspace." https://drone-detection-system.com.

[2] "Addressing the Growing Threat of Drones with Confidence." https://aaronia.com/en/news/post/confidently-countering-the-threat-posed-by-drones.

[3] "AARTOS CMS Jammer." https://kbsecuritytraining.com/aartos-cms-jammer.

[4] S. Magnuson. "EUROSATORY NEWS: Kongsberg's Counter-Drone 'Secret Sauce' Refined in Ukraine." https://www.nationaldefensemagazine.org/articles/2024/6/18/kongsbergs-counter-drone-secret-sauce-refined-in-ukraine. June 2024.

[5] "Kongsberg Aims to Enhance US Army's CROWS Remote Weapon Stations with C-UAS Capability at AUSA 2025." https://news.defcros.com/kongsberg-aims-to-enhance-us. Oct. 25.

[6] "DR 100 for C-UAS." https://www.kongsberg.com/discovery/surveillance-monitoring/dr/dr100-c-uas.

[7] G. Olfert. "Kongsberg to Integrate Counter-UAS Capability into US Army's CROWS Remote Weapon Stations." https://milivox.media/kongsberg-crows-counter-uas-upgrade. Oct. 2025.

[8] "Breaking the Kill Chain: Multi-Domain Operations Against A2AD." https://www.europeafrica.army.mil/Home/LANDEURO/LANDEURO-ARTICLE-View/Article/4115410/breaking-the-kill-chain-multi-domain-operations-against-a2ad. Mar. 25.

[9] C. Barron. "Drone Comms in GPS-Denied Environments: Tactical Mesh Solutions." https://www.bluwireless.com/insight/gps-denied-drone-communications.

[10] E. Niewood, S. Lee, and G. Grant, "Envisioning a New Command & Control (C2) Architecture For All-Domain Operations," MITRE, Rep. 20-3263, Feb. 2021.

[11] "Operation Spiderweb." https://en.wikipedia.org/wiki/Operation_Spiderweb.

[12] "Operation Spiderweb: Covert Drone Strike Inside Russia." https://www.janes.com/osint-insights/defence-and-national-security-analysis/operation-spiderweb-ukraine-covert-drone-strike-inside-russia. June 25.

[13] L. Chiu. "Russia Hits Truck Drivers in Devastating 'Operation Spider' With Terrorism Charges." https://www.kyivpost.com/post/69053. Jan. 2026.

[14] "Delving into 'Operation Spider's Web': Precision strikes in depth on Russian air bases." https://tochnyi.info/2025/06/a-deep-dive-into-operation-spiderweb-precision-strike-in-depth-on-russian-air-bases. June 25.

[15] M. Collett-White, P. K. Dutta, and M. Zafra. "Russia Hits Truck Drivers in Devastating 'Operation Spider' With Terrorism Charges." https://www.reuters.com/graphics/UKRAINE-CRISIS/DRONES-RUSSIA/mypmjzayyvr. June 25.

[16] K. Bondar. "How Ukraine's Operation 'Spider's Web' Redefines Asymmetric Warfare." https://www.csis.org/analysis/how-ukraines-spider-web-operation-redefines-asymmetric-warfare. June 25.

[17] M. Zafra and J. McClure. "Sea drones and the counteroffensive in Crimea." https://www.reuters.com/graphics/UKRAINE-CRISIS/CRIMEA/gdvzwrmrlpw. June 25.

[18] M. Kubala. "A Closer Look At The Special Sea Drones Used To Pull Off The Crimea Bridge Attack." https://worldcrunch.com/focus/russia-ukraine-war/sea-drones-kerch-bridge-ukraine. July 23.

[19] H. Kesteloo. "Ukraine's Upgraded Sea Baby Drone Now Strikes Anywhere In Black Sea, Forces Russian Fleet Retreat." https://dronexl.co/2025/10/24/ukraine-upgraded-sea-baby-drone. Oct. 25.

[20] L. J. M. Mazzucco. "How Ukraine's Unmanned Surface Vessels Have Reshaped Modern Naval Warfare in the Black Sea." https://rsdi.ae/en/publications/how-ukraines-unmanned-surface-vessels-have-reshaped-modern-naval-warfare-in-the-black-sea. Oct. 25.

[21] D. Mykhailenko. "Meet the New "Sea Baby" Drones Behind the Attack on the Crimean Bridge." https://united24media.com/latest-news/ukraine-unleashes-missile-ready-sea-baby-drones-to-hunt-russias-black-sea-fleet-12702. Oct. 25.

[22] Y. Taradiuk. "SBU reveals next-gen Sea Baby naval drones, confirms use in June Crimea Bridge attack." https://kyivindependent.com/sbu-releases-new-baby-sea-drones-confirms-it-was-used-in-an-attack-on-sea-bridge. Oct. 25.

[23] P. Yana. "SBU shows new generation of maritime drones: They hit Crimean bridge in summer – photos." https://news.liga.net/en/society/news/sbu-shows-new-generation-of-maritime-drones-they-hit-crimean-bridge-in-summer—photos. Oct. 25.

[24] H. Altman. “Ukraine’s Uncrewed Surface Vessels Are Now Launching Bomber Drones To Attack Crimea.” https://www.twz.com/news-features/ukraines-uncrewed-surface-vessels-are-now-launching-bomber-drones-to-attack-crimea. June 25.

[25] J. E. Kline. “A Tactical Doctrine for Distributed Lethality.” https://cimsec.org/tactical-doctrine-distributed-lethality. Feb. 16.

[26] “CODE: Collaborative Operations in Denied Environment.” https://www.darpa.mil/research/programs/collaborative-operations-in-denied-environment.

[27] M. A. Lopez, M. Baddeley, W. T. Lunardi, A. Pandey, and J.-P. Giacalone, “Towards Secure Wireless Mesh Networks for UAV Swarm Connectivity: Current Threats, Research, and Opportunities,” July 2021. Available: https://doi.org/10.48550/arXiv.2108.13154

[28] Y. Alqudsi and M. Makaraci, “UAV swarms: Research, challenges, and future directions,” *Journal of Engineering and Applied Science*, vol. 72, no. 1, p. 12, Dec. 2025. Available: https://doi.org/10.1186/s44147-025-00582-3

[29] L. Davoli, E. Pagliari, and G. Ferrari, “Hybrid LoRa-IEEE 802.11s Opportunistic Mesh Networking for Flexible UAV Swarming,” *Drones*, vol. 5, no. 2, p. 26, Apr. 2021. Available: https://doi.org/10.3390/drones5020026

[30] M. A. Hamza, M. Mohsin, M. Khalil, and S. M. Kazam Abbas Kazmi, “MAVLink Protocol: A Survey of Security Threats and Countermeasures,” in *2024 4th International Conference on Digital Futures and Transformative Technologies (ICoDT2)*. Islamabad, Pakistan: IEEE, Oct. 2024, pp. 1–8. Available: https://doi.org/10.1109/ICoDT262145.2024.10740195

[31] V. Nazarenko. “1,100 kg twice: SBU Head reveals explosive details of third Crimean Bridge attack.” https://www.msn.com/en-us/news/world/1100-kg-twice-sbu-head-reveals-explosive-details-of-third-crimean-bridge-attack/ar-AA1HgtVX. June 25.

[32] P. Yue *et al.*, “UAV Autonomous Navigation System Based on Air–Ground Collaboration in GPS-Denied Environments,” *Drones*, vol. 9, no. 6, p. 442, June 2025. Available: https://doi.org/10.3390/drones9060442

[33] D. Akhihiero, U. Olawoye, S. Das, and J. Gross, “Cooperative Localization for GNSS-Denied Subterranean Navigation: A UAV–UGV Team Approach,” *NAVIGATION: Journal of the Institute of Navigation*, vol. 71, no. 4, p. navi.677, 2024. Available: https://doi.org/10.33012/navi.677

[34] D. Henley. “US, allies and partners integrate for dynamic targeting kill-chain automation experiments.” https://www.af.mil/News/Article-Display/Article/3663956/us-allies-and-partners-integrate-for-dynamic-targeting-kill-chain-automation-ex. Jan. 24.

[35] A. Wylie. “Anduril Demonstrates AI-Enabled Rapid Targeting Solution.” https://www.defenseadvancement.com/news/andurils-demonstrates-ai-enabled-rapid-targeting-solution. Dec. 23.

[36] “The GS Platform for Defense.” https://www.greensightag.com/defense.

[37] “Quantum Systems.” https://quantum-systems.com/us.

[38] “Trinity Pro.” https://enterprise.dronenerds.com/commercial-drone-platforms/quantum-systems-trinity-pro.

[39] “Twister: Smart short-range eVTOL sUAS.” https://quantum-systems.com/twister.

[40] M. Chomsky. “Quantum Systems wins Bundeswehr contract to supply Twister drones as ALADIN successor system.” https://defence-industry.eu/quantum-systems-wins-bundeswehr-contract-to-supply-twister-drones-as-aladin-successor-system. Dec. 25.

[41] “Quantum Systems wins German Armed Forces tender for ALADIN successor.” https://www.suasnews.com/2025/12/quantum-systems-wins-german-armed-forces-tender-for-aladin-successor. Dec. 2025.

[42] “DX Series Breadcrumbs.” https://rajant.com/products/dx-series.

[43] “Rajant DX2-50 BreadCrumb Radio.” https://www.borderstates.com/All-Products/Communications-DataComm/Wireless-Cellular/Wireless-Radios-Controllers/Rajant-DX2-50-BreadCrumb-Radio/Rajant-DX2-50-BreadCrumb-Radio/p/3481352.

[44] P. Chandra, D. M. Dobkin, D. Bensky, R. Olexa, D. Lide, and F. Dowla, *Wireless Networking: Know It All*, 1st ed. Amsterdam: Elsevier/Newnes, Sep. 2007.

[45] S. K. Huo *et al.*, “An Analysis of the UAV Relay Coverage in Mobile Ad-Hoc Network,” *Applied Mechanics and Materials*, vol. 577, pp. 879–883, July 2014. Available: https://doi.org/10.4028/www.scientific.net/AMM.577.879

[46] W. Heinzelman, A. Chandrakasan, and H. Balakrishnan, “An application-specific protocol architecture for wireless microsensor networks,” *IEEE Transactions on Wireless Communications*, vol. 1, no. 4, pp. 660–670, Oct. 2002. Available: https://doi.org/10.1109/TWC.2002.804190

[47] M. Aslam, N. Javaid, A. Rahim, U. Nazir, A. Bibi, and Z. A. Khan, "Survey of Extended LEACH-Based Clustering Routing Protocols for Wireless Sensor Networks," 2012. Available: https://doi.org/10.48550/ARXIV.1207.2609

[48] M. Al-Shalabi, M. Anbar, T.-C. Wan, and A. Khasawneh, "Variants of the Low-Energy Adaptive Clustering Hierarchy Protocol: Survey, Issues and Challenges," *Electronics*, vol. 7, no. 8, p. 136, Aug. 2018. Available: https://doi.org/10.3390/electronics7080136

[49] Kamel Tebessi and Fouzi Semchedine, "An Improvement on LEACH-C Protocol (LEACH-CCMSN)," *Automatic Control and Computer Sciences*, vol. 56, no. 1, pp. 10–16, Feb. 2022. Available: https://doi.org/10.3103/S0146411622010102

[50] S. Sennan, S. Ramasubbareddy, R. K. Dhanaraj, A. Nayyar, and B. Balusamy, "Energy-efficient cluster head selection in wireless sensor networks-based internet of things (IoT) using fuzzy-based Harris hawks optimization," *Telecommunication Systems*, vol. 87, no. 1, pp. 119–135, Sep. 2024. Available: https://doi.org/10.1007/s11235-024-01176-9

[51] S. Aramuthakannan, R. Raja Kumar, G. Mariammal, and M. Geetha, "Enhanced Cluster Head Selection and Routing in Wireless Sensor Networks Using Fuzzy Logic and Adaptive Cat Swarm Optimization," *International Journal of Intelligent Engineering and Systems*, vol. 17, no. 1, pp. 721–731, Feb. 2024. Available: https://doi.org/10.22266/ijies2024.0229.61

[52] S. I. Hamim and A. B. A. Rahman, "Optimizing Wireless Sensor Networks: A Survey of Clustering Strategies and Algorithms," *International Journal of Computer Networks and Applications*, vol. 11, no. 5, pp. 673–689, Oct. 2024. Available: https://doi.org/10.22247/ijcna/2024/42

[53] M. C. M. Thein and T. Thein, "An Energy Efficient Cluster-Head Selection for Wireless Sensor Networks," in *2010 International Conference on Intelligent Systems, Modelling and Simulation*. Liverpool, United Kingdom: IEEE, Jan. 2010, pp. 287–291. Available: https://doi.org/10.1109/ISMS.2010.60

[54] S. A. Engebråten, J. Moen, O. Yakimenko, and K. Glette, "Evolving a Repertoire of Controllers for a Multi-function Swarm," in *Applications of Evolutionary Computation*, K. Sim and P. Kaufmann, Eds. Cham: Springer International Publishing, 2018, vol. 10784, pp. 734–749. Available: https://doi.org/10.1007/978-3-319-77538-8_49

THIS PAGE INTENTIONALLY LEFT BLANK

Initial Distribution List

1. Defense Technical Information Center
   Fort Belvoir, Virginia

2. Dudley Knox Library
   Naval Postgraduate School
   Monterey, California

3. Naval Research Program
   Naval Postgraduate School
   Monterey, California